Renewable and Sustainable Energy Reviews 40 (2014) 688–715

Contents lists available at ScienceDirect

Renewable and Sustainable Energy Reviews

journal homepage: www.elsevier.com/locate/rser

Advances in mathematical modeling of fluidized bed gasification

Chanchal Loha [a,*], Sai Gu [b], Juray De Wilde [c], Pinakeswar Mahanta [d], Pradip K. Chatterjee [a]

[a] Thermal Engineering Group, CSIR – Central Mechanical Engineering Research Institute, Durgapur 713209, India
[b] School of Engineering, Cranfield University, Cranfield, Bedfordshire MK43 0AL, England
[c] Materials and process engineering (IMAP), UCL, Place Sainte Barbe 2 bte L5.02.02 à, 1348 Louvain-la-Neuve, Belgium
[d] Mechanical Engineering Department, Indian Institute of Technology Guwahati, Guwahati 781039, Assam, India

ARTICLE INFO

Article history:
Received 14 November 2013
Received in revised form
18 July 2014
Accepted 30 July 2014

Keywords:
Gasification
Fluidized bed
Euilibrium model
Two-phase flow model
Euler–Euler model
Euler–Lagrange model

ABSTRACT

Gasification is the thermochemical conversion of solid fuel into the gas which contains mainly hydrogen, carbon monoxide, carbon dioxide, methane and nitrogen. In gasification, fluidized bed technology is widely used due to its various advantageous features which include high heat transfer, uniform and controllable temperature and favorable gas–solid contacting. Modeling and simulation of fluidized bed gasification is useful for optimizing the gasifier design and operation with minimal temporal and financial cost. The present work investigates the different modeling approaches applied to the fluidized bed gasification systems. These models are broadly classified as the equilibrium model and the rate based or kinetic model. On the other hand, depending on the description of the hydrodynamic of the bed, fluidized bed models may also be classified as the two-phase flow model, the Euler–Euler model and the Euler–Lagrange model. Mathematical formulation of each of the model mentioned above and their merits and demerits are discussed. Detail reviews of different model used by different researchers with major results obtained by them are presented while the special focus is given on Euler–Euler and Euler–Lagrange CFD models.

Contents

* Corresponding author.
E-mail address: chanchal.loha@gmail.com (C. Loha).

http://dx.doi.org/10.1016/j.rser.2014.07.199
1364-0321/

1. Introduction and objective

The rapid growth in industrialization all over the world with simultaneous increase in population, air pollution has reached a very critical level, which threatens the public health, deteriorates the environment and damages property and landscape. An alarming deterioration of the quality of the life nullified the advantages gained by a rise in living standards due to industrial development. The problem became so serious that over the last few decades all industrialized and some developing countries introduced increasingly stringent legislation, restricting permissible levels of pollutant emission from major combustion systems such as electricity generating power stations, furnaces and industrial plants as well as by automobiles and aircrafts. Therefore, the conservation of limited supply of fossil fuel, climate change and the increasing concern over global warming prompted a search for a new and clean technology. Amongst the different technologies, one of the most promising future energy technologies is the fluidized bed gasification.

Gasification is the thermochemical conversion of solid fuel into the fuel gas which contains mainly hydrogen, carbon monoxide, carbon dioxide, methane and nitrogen. The product gas from the reactor also contains some contaminants like char particle, ash and some higher hydrocarbons or tar. A limited supply of oxygen, air, steam or a combination of these serves as gasifying agent. The gasification consists of four different steps e.g. drying, pyrolysis or devolatilization, combustion or oxidation and gasification or reduction. These four steps are described below.

1.1. Drying

Drying occurs at about 100–200 °C when the moisture from the solid fuel is driven out and converted into vapor. The solid fuel in this stage is not decomposed because the temperature is not high enough to cause any chemical reaction.

1.2. Pyrolysis or devolatilization

This is a thermal decomposition process where the dried solid fuel is decomposed into low to high molecular weight volatiles including tar and solid charcoal in the absence of oxygen. The pyrolysis or devolatilization reactions are endothermic and thus the heat needed for these reactions is supplied from the combustion or oxidation reactions.

1.3. Combustion or oxidation

The products of the pyrolysis or devolatilization process are partially oxidized by oxygen supplied through air, and then from carbon monoxide, carbon dioxide and water vapor or steam. As the combustion reactions are exothermic and other reactions in gasification are endothermic, the overall heat required for endothermic reactions is supplied by this combustion or oxidation process.

1.4. Gasification or reduction

In gasification step several reduction reactions occur in absence of oxygen because oxygen is consumed in the combustion reactions. These reduction reactions are mostly endothermic. The final products from these reactions are mainly gas mixtures including hydrogen, carbon monoxide, carbon dioxide and methane.

Most of the time drying, pyrolysis or devolatilization, combustion or oxidation and gasification or reduction steps are not separated but they are overlapped in gasification process. For example, in case of large particle, these steps can take place simultaneously. When the large particle is heated up, the outside portion is dried and devolatization also starts. In the core, the particle is still cooler. When the center of a large particle is heated up, too, and drying and devolatization already started on the outside of the particle, the residual char is likely to be already gasified.

In order to investigate the gasification process, different types of gasifiers are developed like updraft gasifier, downdraft gasifier, cross draft gasifier, bubbling fluidized bed gasifier, circulating fluidized bed gasifier, twin fluidized bed gasifier, entrained flow gasifier etc. Detailed descriptions of the gasification technologies are available in the literature [1,2]. Amongst the different types of gasification technologies, the fluidized bed technology has a number of advantages which include but not limited to the high heat transfer, uniform and controllable temperature, favorable gas–solid contacting, higher efficiency and fuel flexibility.

In order to analyze the process of fluidized bed gasification, several modeling approaches have been deployed and they are broadly classified into two groups; equilibrium modeling and rate base or kinetic modeling. Equilibrium modeling is independent of the type of gasifier because it does not consider the hydrodynamic of the bed. Depending upon the process of calculating the product gas composition, the equilibrium model may be classified as the stoichiometric equilibrium model or non-stoichiometric equilibrium model. Whereas, the kinetic model generally consider the hydrodynamics of the bed coupling with the reaction kinetics. Based on the hydrodynamic modeling, the fluidized bed models can also be classified as two-phase flow model, Euler–Euler model and Euler–Lagrange model. In hydrodynamic modeling, the most established model is the two-phase flow model. Very recently, the computational fluid dynamic (CFD) modeling of fluidized bed gasification based on Euler–Euler approach and Euler–Lagrange approach are attempted by researchers due to the increasing computational power of the modern computers. But, application of CFD model to study the fluidized bed gasification process is in the developing stage and more studies are needed [3,4]. In the present work, a detailed review of different fluidized bed gasification models published in the literature is presented. Mathematical equations governing fluid and solid flow, heat and mass transfer and chemical reactions for each model are presented. Advantages and disadvantages of different modeling approaches and major results obtained are discussed. The special attention has been given to the recently published Euler–Euler and Euler–Lagrange CFD models.

2. Fluidized bed gasifiers

There are different types of fluidized bed gasifiers reported in the literature. Amongst them, a detailed description of the bubbling fluidized bed gasifier, the circulating fluidized bed gasifier and the twin fluidized bed gasifier are presented here. Fig. 1 shows the

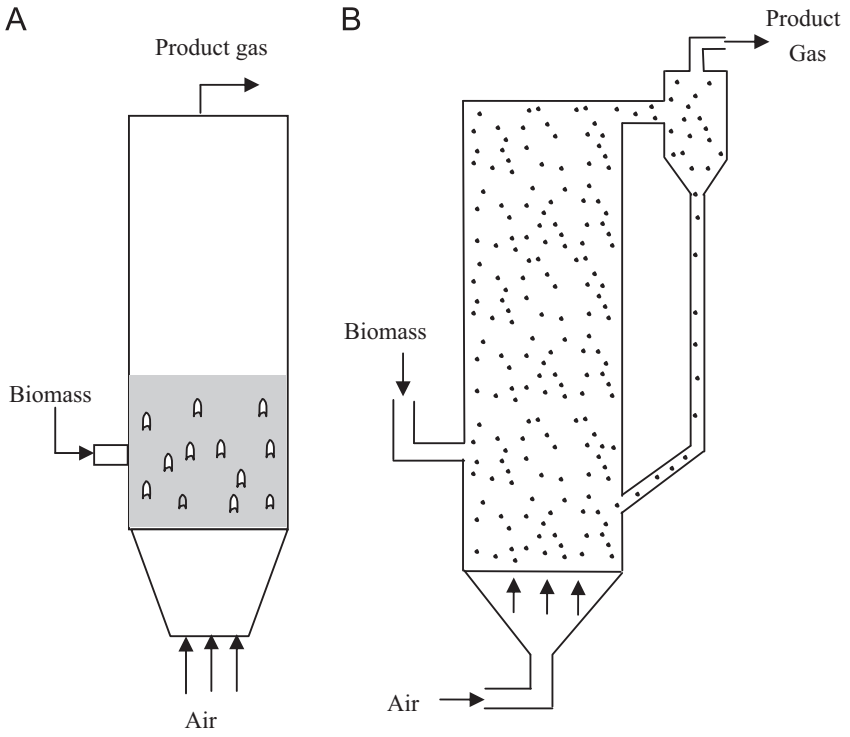

Fig. 1. Schematic diagram of (A) bubbling fluidized bed gasifier and (B) circulating fluidized bed gasifier.

schematic diagram of bubbling, circulating and twin fluidized bed gasifiers.

2.1. Bubbling fluidized bed gasifier

In a typical gasifier, when the gas velocity is increased, a situation is reached when the particles are just suspended in the upward flowing gas. At this situation the frictional force between a particle and fluid counterbalance the weight of particle, the vertical component of the compressive force between adjacent particles disappears and the pressure drop through any section of the bed equals the weight of fluid and particles in that section. At this instance, the bed is considered to be at minimum fluidization condition. With an increase in velocity beyond the minimum fluidization velocity, large instabilities with bubbling and channeling of the gas are observed. At higher flow rates agitation becomes more violent and the movement of solids becomes more vigorous. However, the bed does not expand much beyond its volume at minimum fluidization. Such a bed is called bubbling fluidized bed (Fig. 1A). In a bubbling fluidized bed, gas moves through the bed in void and in bubbles with higher velocity. Some of the particles are entrained into the freeboard along with these fast moving bubbles and some fine particles are transported with the product gas and leave the reactor at the top. But most of the entrained particles fall back and can be continuously removed from the fluidized bed with the remaining ash at the bottom. The bubbling fluidized bed gasifiers have a number of advantages over non-fluidized bed gasifiers which include fuel flexibility, uniform temperature, higher efficiency, lower capital and maintenance cost etc.

2.2. Circulating fluidized bed gasifier

When the gas velocity is increased further, beyond the bubbling fluidized bed regime, the solids will be distributed across the whole riser height and entrained by the gas at the top of the gasifier. Particles are separated from the gas in a cyclone and are returned to the fluid bed near the bottom. Then it becomes a

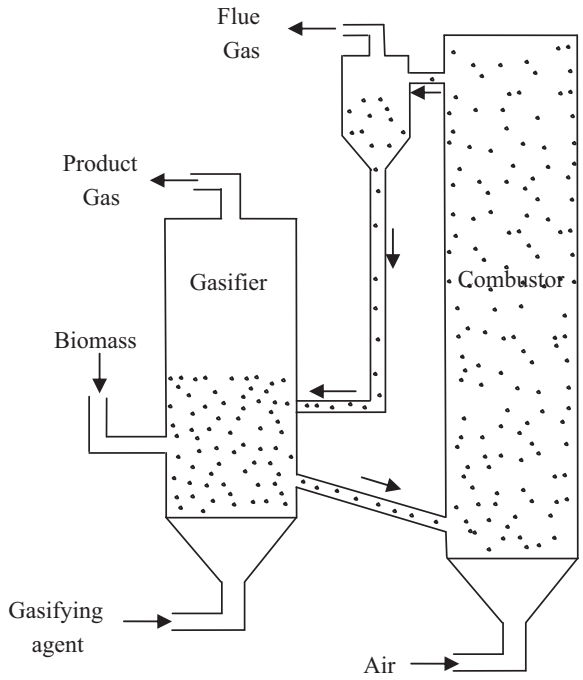

Fig. 2. Schematic diagram of a twin fluidized bed gasifier.

circulating fluidized bed (Fig. 1B). The advantage of circulating fluidized beds in mainly due to the longer overall residence time. The solids circulate in the outer loop, going up in the riser, leaving at the top, going down in the return leg and entering the riser again at the bottom. But there is also internal circulation of the solids, which fall back from the higher region of the riser and move downwards at the riser wall. Circulating fluidized bed gasifiers are normally used for large applications. It has enhanced flexibility over bubbling fluidized bed gasifier for firing multi-fuels with high moisture content and significantly higher efficiency.

2.3. Twin-fluidized bed gasifier

Another form of fluidized bed gasifier which is also reported in the literature is the twin fluidized bed gasifier as shown in Fig. 2. In one fluidized bed (generally bubbling) the gasifying agent (mostly steam) is brought into contact with the fuel fed to this fluidized bed. There is continuous discharge of bed material with unreacted char particles from this first fluidized bed, which is then fed to a second fluidized bed (generally circulating) operated with air and used as a combustor to burn the remaining char and to heat the fluid bed particles. Then the hot bed material from the second fluidized bed is circulated to the first fluidized bed to supply the heat for the endothermic steam gasification reactions. This technology is especially interesting for biomass gasification due to the higher volatiles content in the biomass compared to coal. Here only the volatiles are used for synthesis of gas production. The fixed carbon content is burned to supply the heat. Therefore, the slow gasification reactions of fixed carbon with steam or carbon dioxide are avoided. Another advantage is that if steam is used in the first fluidized bed, the producer gas is not diluted by nitrogen from the air.

3. Reaction mechanism and kinetics

Mathematical modeling of fluidized bed systems can broadly be classified into two groups; thermodynamic equilibrium model and rate base or kinetic model as described in details below.

3.1. Equilibrium model

The parametric study and the thermodynamic analysis of the gasification process by using equilibrium model is a popular method because it provides a useful design aid in evaluating the possible limiting behavior of a complex reacting system and also it is computationally inexpensive. Though, it is independent of gasifier design, still it can provide a guideline for process design, evaluation and improvement. It can also be used to study the influence of most important process parameters. For this reason many authors used the thermodynamic equilibrium mode to study the fluidized bed gasification process.

Equilibrium models are generally developed based on following assumptions:

- The process occurs at steady state.
- The gasifier is isothermal and at equilibrium condition.
- Reaction rates are fast enough and residence time is sufficient to reach equilibrium condition.
- Gases except H_2, CO, CO_2 and CH_4, N_2 and H_2O are negligible.
- Char contains only solid carbon.
- Ash residue is negligible.
- The product gas is at the gasifier temperature.
- All the gases obey the ideal gas law.
- Potential and kinetic energies are negligible.

There are two general approaches for equilibrium modeling viz. stoichiometric equilibrium model and non-stoichiometric equilibrium model. However, both approaches are conceptually similar [5], they differs. The detailed description of stoichiometric equilibrium model and non-stoichiometric equilibrium model is presented below.

3.1.1. Stoichiometric equilibrium model

The stoichiometric equilibrium model is based on selecting those species which are present in the largest amounts, i.e. those species having the lowest value of Gibbs free energy of formation. It requires a clearly defined reaction mechanism that incorporates all chemical reactions and species involved. It uses the elemental balance and the equilibrium constants of selected reactions. A stoichiometric equilibrium model may also use Gibbs free energy data to determine the equilibrium constants of a propose set of reactions.

A brief description of stoichiometric equilibrium model based on the work of Loha et al. [6,7] is given below. In stoichiometric equilibrium model, the gasification process is represented by a global gasification reaction as follows:

$$CH_xO_y + wH_2O + mH_2O = \gamma_{H_2}H_2 + \gamma_{CO}CO + \gamma_{CO_2}CO_2 + \gamma_{H_2O}H_2O + \gamma_{CH_4}CH_4 \quad (1)$$

where CH_xO_y represents the solid fuel which contains carbon, hydrogen and oxygen. Other elements are neglected. Here, x and y represent numbers of atoms of hydrogen and oxygen per number of atom of carbon in the solid fuel and can be obtained from the ultimate analysis of the solid fuel, w is the mole of moisture per mole of dry ash free solid fuel and m is the mole of steam added per mole of dry ash free biomass. On the left hand side all are inputs. On the right hand side, γ_{H_2}, γ_{CO}, γ_{CO_2}, γ_{H_2O} *and* γ_{CH_4} are the numbers of mole of gas species on the product gas and which are obtained by solving material balance and equilibrium constant equations of selected reactions. The material balance equations of carbon, hydrogen and oxygen are given below.

Carbon balance

$$1 = \gamma_{CO} + \gamma_{CO_2} + \gamma_{CH_4} \quad (2)$$

Hydrogen balance

$$x + 2w + 2m = 2\gamma_{H_2} + 2\gamma_{H_2O} + 4\gamma_{CH_4} \quad (3)$$

Oxygen balance

$$y + w + m = \gamma_{CO} + 2\gamma_{CO_2} + \gamma_{H_2O} \quad (4)$$

Now, it is required to select the major chemical reactions for calculating the product gas composition. For the present calculation following reactions are selected.

$$\text{Water} - \text{gas shift reaction} \quad CO + H_2O = CO_2 + H_2 \quad (5)$$

$$\text{Methane reaction}: \quad C + 2H_2 = CH_4 \quad (6)$$

All gases are assumed to be ideal and all reactions form at atmospheric pressure. Therefore, the equilibrium constants of the above two reactions, which are functions of temperature, are given below.

The equilibrium constant of water–gas shift reaction is

$$K_1 = \frac{P_{CO_2}P_{H_2}}{P_{CO}P_{H_2O}} = \frac{x_{CO_2}x_{H_2}}{x_{CO}x_{H_2O}} \quad (7)$$

where x_i is the mole fraction of the gas species $i$in the gas mixture, $x_i = \gamma_i/\gamma_{total}$ and here

$\gamma_{total} = \gamma_{H_2} + \gamma_{CO} + \gamma_{CO_2} + \gamma_{H_2O} + \gamma_{CH_4}$.

The equilibrium constant for methane formation reaction is

$$K_2 = \frac{P_{CH_4}}{(P_{H_2})^2} = \frac{x_{CH_4}}{(x_{H_2})^2} \quad (8)$$

Equilibrium constant K is a function of temperature and can directly be obtained from JANAF thermochemical tables [8] or can be calculated from the Gibbs function as given below.

$$\ln K = -\frac{\Delta G_T^o}{\overline{R}T} \quad (9)$$

$$\Delta G_T^o = \sum_i \gamma_i \, \Delta \overline{g}_{f,T,i}^o \quad (10)$$

where $\overline{R}$ is the universal gas constant, ΔG_T^o is the standard Gibbs function of reaction and $\Delta\overline{g}^o_{f,T,i}$ represents the standard Gibbs function of formation at given temperature T (K) of the gas species i which can be expressed by the empirical equation given below:

$$\Delta\overline{g}^o_{f,T} = \overline{h}^o_f - aT\ln(T) - bT^2 - \frac{c}{2}T^3 - \frac{d}{3}T^4 + \frac{e}{2T} + f + gT \tag{11}$$

The values of coefficients a–g and the enthalpy of formation ($\overline{h}^o_f$) of different gases are available in the literature [9].

3.1.2. Non-stoichiometric equilibrium model

The non-stoichiometric equilibrium model is based on the minimization of Gibbs free energy of the system without specification of the possible reactions taking place. Here, only the elemental composition of the fuel is needed to specify which can be obtained from the ultimate analysis of the fuel. This method is particularly suitable for problems with unclear reaction mechanisms. A non-stoichiometric equilibrium modeling approach based on the literature [10,11] is presented below. The model is based on the RAND [12,13] algorithm. Here, the change in mole of a species in the mth iteration can be expressed explicitly as a function of its current chemical potential, the phase distribution of the species at a given system temperature and pressure and the Lagrange multiplier as given below:

$$\begin{aligned}\delta n_i^{(m)} &= n_i^{(m)}\left(\sum_{k=1}^{K} a_{ik}\psi_k + u_\alpha - \frac{\mu_i^{(m)}}{RT}\right) \quad \text{for multi} - \text{species phase}\\ &= u_\alpha n_i^{(m)} \qquad\qquad\qquad\qquad \text{for single} - \text{species phase}\\ &(i = 1,2,\ldots,N; \quad k = 1,2,\ldots,K; \quad \alpha = 1,2,\ldots,\pi)\end{aligned} \tag{12}$$

Here, N denotes the total number of species, $n_i^{(m)}$ denotes the mole of species i in the mth iteration, a_{ik} is the coefficient in species-element matrix, $\mu_i^{(m)}$ is the chemical potential of species i in the mth iteration, ψ_k is a function related to Lagrange multiplier λ_k and u_α is the phase split of $\delta n_i^{(m)}$.

Here, ψ_k is given by

$$\psi_k = \frac{\lambda_k}{RT} \tag{13}$$

and u_α is given by

$$u_\alpha = \sum_{i=1}^{N} \delta n_{i\alpha}^{(m)} / n_t^{(m)} = \delta n_{t\alpha}^{(m)} / n_t^{(m)} \tag{14}$$

where subscript t means total and α refers to the phase to which a species belongs.

Therefore, a set of $(K+\pi)$ simultaneous algebraic equations that are to be solved iteratively by the RAND algorithm includes K linear equations regarding element abundance

$$\begin{aligned}&\sum_{k=1}^{K}\sum_{i=1}^{N} a_{ik}a_{ij}n_i^{(m)}\psi_k + \sum_{\alpha=1}^{\pi} b_{j\alpha}^{(m)}u_\alpha = \sum_{i=1}^{N} a_{ij}n_k^{(m)}\frac{\mu_i^{(m)}}{RT} + b_k - b_k^{(m)}\\ &(j = 1,2,\ldots,K)\end{aligned} \tag{15}$$

and π supplementary equations for different phases

$$\begin{aligned}&\sum_{k=1}^{K} b_{k\alpha}^{(m)}\psi_k - n_{z\alpha}u_\alpha = \sum_{i=1}^{N} n_{i\alpha}^{(m)}\frac{\mu_{i\alpha}^{(m)}}{RT}\\ &(\alpha = 1,2,\ldots,\pi)\end{aligned} \tag{16}$$

The initial elemental abundance vector b is calculated from the feedstock and the kth element of the b vector at the mth iteration is

$$b_k^{(m)} = \sum_{i=1}^{N} a_{ik}n_i^{(m)} \tag{17}$$

Mass balance constraints are imposed at every iterations during solution of above equations, while the algorithm iteratively minimizes the Gibbs free energy. The difference between the initial elemental abundance vector and its current iteration value ($b_k - b_k^{(m)}$), is added to the right hand side of Eq. (15) to eliminate error accumulation during the iteration process [14].

Finally, the new numbers of moles vector, $\mathbf{n}^{(m+1)}$, is determined by

$$\mathbf{n}^{(m+1)} = \mathbf{n}^{(m)} + \omega^{(m)}\delta\mathbf{n}^{(m)} \tag{18}$$

where $\omega^{(m)}$ is the step size parameter.

Finally, the molar fractions of all species are determined by

$$x_i = \frac{n_i}{n_t} \tag{19}$$

Equilibrium models are extensively used by many authors [15–23] due to its advantageous feature of simplicity and it gives quick idea of limits of operation compared to the rate base model. It can provide the final gas composition variation with operating condition, gas yield, calorific value of gas, carbon conversion etc. The prediction using equilibrium model matches well with the experiment when the equilibrium condition is prevailed i.e. when the rate of reaction is very fast compared to the residence time of reactants in the gasifier. The equilibrium model cannot predict the spatial variation of the product inside the gasifier as well as the temporal variation. It is also important to note that the predicted methane concentration from equilibrium model is always substantially lower than the experimentally observed data for gasification process. The high amount of methane in the experimental gas composition is a non-equilibrium species resulting from pyrolysis reactions and limited char gasification is achieved in the gasifier. So, the measured gas composition is largely attributed to pyrolysis which the equilibrium model cannot account for. The equilibrium model cannot predict highly accurate result for fluidized bed gasifier due to its inherent assumptions. The residence time, feed configuration, internal mixing and gas–solid contacting pattern in fluidized bed gasifier account for large deviation.

Thus, in order to predict more accurately the behavior of fluidized bed gasifier, different modifications of the existing equilibrium models have been done as discussed below. Li et al. [10,11] modified their non-stoichiometric equilibrium model by introducing the experimental carbon conversion from fluidized bed gasification and got better agreement to the experimental data. For example, they compared the higher heating value (HHV) of the product gas as a function of air ratio from experiment, pure equilibrium model and modified equilibrium model as shown in Fig. 3. It was observed that the modified equilibrium model

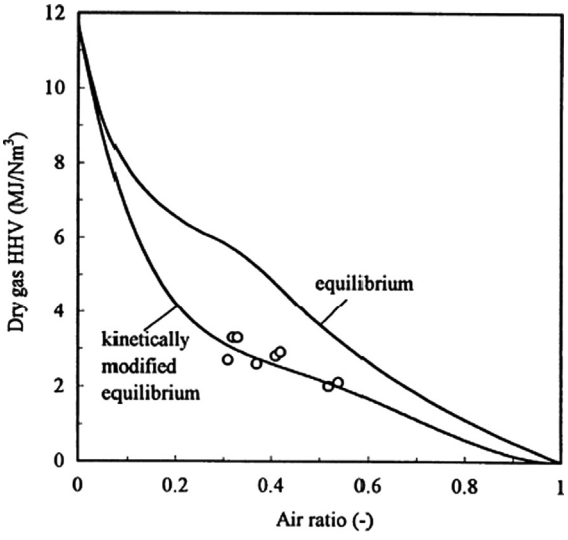

Fig. 3. Effect of air ratio on dry gas HHV for as-received high value coal gasified at 155 kPa and 1020–1150 K. Points are experimental value [9].

Table 1
Gas composition by using pure equilibrium model and modified equilibrium model and experiment [5].

Tempe (°C)	S/B	Experiment				Pure equilibrium model				RMS error	Modified equilibrium model				RMS error
		H_2	CO	CO_2	CH_4	H_2	CO	CO_2	CH_4		H_2	CO	CO_2	CH_4	
690	1.32	50.50	14.30	26.60	8.60	48.76	12.99	31.21	7.03	2.667429	48.4	16.26	28.88	6.46	2.123064
730	1.32	52.20	16.40	23.50	7.90	50.71	15.48	28.74	5.06	3.10603	50.14	18.94	26.33	4.6	2.720023
750	1.00	49.50	23.70	21.20	5.60	50.37	20.59	25.01	4.02	2.619232	49.64	24.22	22.52	3.62	1.219918
750	1.32	52.30	17.75	22.25	7.40	51.43	16.64	27.65	4.28	3.197006	50.76	20.15	25.22	3.87	2.711706
750	1.70	52.90	16.40	22.90	7.80	52.26	13.50	29.74	4.50	4.077229	51.67	16.78	27.47	4.08	3.015817
770	1.32	54.40	18.50	19.40	7.70	52.00	17.72	26.66	3.62	4.350931	51.24	21.28	24.23	3.25	3.900173
						Average RMS				**3.33631**	Average RMS				**2.615117**

predicted the experimental values much better than the pure equilibrium model. Loha et al. [6] studied the fluidized bed biomass gasification by using a stoichiometric equilibrium model. The pure equilibrium model was modified by multiplying equilibrium constants with pre factors. Results from the pure equilibrium model, the modified equilibrium model and the experiment were compared as shown in Table 1. It was observed that average RMS error reduced from 3.33631 to 2.615117 while using the modified equilibrium model. Fryda et al. [24] and Schuster et al. [25] also evaluated the product gas composition from fluidized bed gasification by using equilibrium model. They modified the equilibrium model by introducing the un-reacted char carbon as some percentage of the biomass carbon input and got better agreement to the experimental data.

Therefore, if the equilibrium model is modified, it can be use to study the fluidized bed gasification performance, particularly to study the influence of most important parameters on the overall performance. Equilibrium model also provides the thermodynamic limits of the gasification system. Hence, the equilibrium model may be useful for preliminary design and comparison of fluidized bed gasification process if they are modified as mentioned above. But, it cannot provide highly accurate data for all cases because it does not consider the hydrodynamic behavior of the system as well as the reaction kinetics. Hence, to get more accurate data for detail design, the rate base modeling or kinetic modeling with hydrodynamic consideration of the fluidized bed system is required as discussed in the following sections.

3.2. Rate base model or kinetic model

Rate base model or kinetic model is more comprehensive and realistic compared to the equilibrium model. It takes into account the hydrodynamics, transport process and reaction kinetics. In rate base model, a detailed reaction mechanism with rate of each reactions are considered depending on the type of fuel used. Modeling the reaction kinetics in gasification process requires the consideration of complex reaction network which consists of pyrolysis, heterogeneous gas–solid reactions and homogeneous gas phase reactions as discussed below.

3.2.1. Pyrolysis

The solid fuel particles undergo pyrolysis upon entering into the hot fluidized bed gasifier. Pyrolysis is basically the decomposition of solid fuel resulting from heat. In gasification, the final product gas composition is important because it determines the heating value of the product gas. Therefore, the kinetic model for total devolatilization, which determines both the extent of produced char and individual char released, should be taken into consideration.

Kinetic models used for determining the pyrolysis product, available in the literature, are either based on a single equation model, two-equation model or a combination of reactions. The single equation model is the simplest one and it is represented as [26]

$$\text{Fuel} \xrightarrow{k} \eta \ \text{volatile} + (1-\eta)\ \text{char} \tag{20}$$

$$k = A \exp\left(\frac{-E}{RT_p}\right) \tag{21}$$

In two equations model, the pyrolysis of any solid fuel is represented by two equations as given below [27]:

$$\text{Fuel} \xrightarrow{k_1} \eta_1 \ \text{volatile} + (1-\eta_1)\ \text{char} \tag{22}$$

$$\text{Fuel} \xrightarrow{k_2} \eta_2 \ \text{volatile} + (1-\eta_2)\ \text{char} \tag{23}$$

where

$$k_i = A \exp\left(\frac{-E_i}{RT_p}\right) \tag{24}$$

Parameters $k$and η in the above equations are to be obtained from experiments. Many publications deal with the calculation of those parameters for various fuels, but there is a great variation between the representations, probably because a number of physical and chemical factors are incorporated in one expression. Despite this fact, this type of expression has been widely used in reactor models due to its simplicity making it computationally tractable, needing only a small set of input data. In most cases, however, it does not give enough information for comprehensive modeling.

The models mentioned above can predict the amounts of volatile and char released during pyrolysis, but the yields of the main gas species are not predicted which also varies with the type of fuel. The pyrolysis gas composition is generally modeled either based on the experimental data available from the literature for a particular fuel [28–30] or based on the developed correlation [31–33]. These correlations are also developed for a particular set of operating conditions and type of fuel which is not always similar to those has to be simulated. Therefore, more fundamental data are desirable to increase the predictive capability of model simulations.

3.2.2. Gasification with air

In case of gasification with air, the heterogeneous reactions of carbon with oxygen in the air are highly exothermic and therefore provide the heat required for the subsequent gasification reactions. The heterogeneous reactions of carbon with oxygen are given below

$$C + O_2 \rightarrow CO_2, \quad \Delta h_R^0 = -393.5\ \text{kJ/mol} \tag{25}$$

$$C + \frac{1}{2}O_2 \rightarrow CO, \quad \Delta h_R^0 = -110.5\ \text{kJ/mol} \tag{26}$$

In addition to the heterogeneous gas–solid reactions, there are also many homogeneous gas phase reactions. These are the combustion reactions of all the gases produced during the pyrolysis step.

The hydrogen and carbon monoxide will be oxidized completely to carbon dioxide and water as given below:

$$H_2+\frac{1}{2}O_2\rightarrow H_2O,\quad \Delta h_R^0=-241.8\ \text{kJ/mol} \tag{27}$$

$$CO+\frac{1}{2}O_2\rightarrow CO_2,\quad \Delta h_R^0=-283.0\ \text{kJ/mol} \tag{28}$$

In addition, the complete combustion of hydrocarbons with oxygen will produce carbon dioxide and water. But, in the reducing atmosphere of gasifier and lack of oxygen, the producs will be hydrogen and carbon monoxide.

$$CH_4+\frac{1}{2}O_2\rightarrow CO+2H_2,\quad \Delta h_R^0=-35.7\ \text{kJ/mol} \tag{29}$$

$$C_2H_4+O_2\rightarrow 2CO+2H_2,\quad \Delta h_R^0=-35.7\ \text{kJ/mol} \tag{30}$$

In gasification, the amount of air added to the gasifier is not sufficient to completely combust the fuel to carbon dioxide and water. Therefore, once all oxygen is consumed, further reaction taking place are homogeneous equilibrium reactions or heterogeneous reactions between char carbon and produced gases so far. Therefore, the gasification with air is basically a combination of steam and carbon dioxide gasification.

3.2.3. Gasification with steam

If steam is used as the gasifying agent or all oxygen in air gasification is consumed, the gasification reactions with steam are the main reactions in the temperature range normally used in fluidized bed. The products of the reactions of solid carbon with steam are hydrogen, carbon monoxide and to a smaller extent also carbon dioxide may be produced.

$$C+H_2O\rightarrow CO+H_2,\quad \Delta h_R^0=+131.3\ \text{kJ/mol} \tag{31}$$

$$C+2H_2O\rightarrow CO_2+2H_2,\quad \Delta h_R^0=+211.4\ \text{kJ/mol} \tag{32}$$

The homogeneous gas phase reaction of steam with methane is given below:

$$CH_4+H_2O\leftrightarrow CO+3H_2\quad \Delta h_R^0=+206.2\ \text{kJ/mol} \tag{33}$$

The very well known water–gas-shift reaction which is independent of the choice of the gasifying agent and operating condition is given below:

$$CO+H_2O\leftrightarrow CO_2+H_2,\quad \Delta h_R^0=-41.2\ \text{kJ/mol} \tag{34}$$

Other homogeneous steam gasification reactions are the reactions of steam with higher hydrocarbons. The main product of these reactions will be other hydrocarbons, carbon monoxide and hydrogen.

3.2.4. Gasification with carbon dioxide

The gasification reaction with carbon dioxide requires higher temperature because this reaction proceeds very slowly. The heterogeneous gasification reaction of carbon dioxide with char carbon is given below:

$$C+CO_2\rightarrow 2CO,\quad \Delta h_R^0=+172.5\ \text{kJ/mol} \tag{35}$$

The homogeneous gas phase reaction of methane with carbon dioxide is given below.

$$CH_4+CO_2\leftrightarrow 2CO+2H_2,\quad \Delta h_R^0=+247.3\ \text{kJ/mol} \tag{36}$$

3.2.5. Other gasification reactions

In addition to the reactions discussed above, there may be some other reactions in the gasification process. For example, the heterogeneous gasification reaction of char carbon with hydrogen is given below. This reaction is significant only at higher pressure:

$$C+2H_2\rightarrow CH_4,\quad \Delta h_R^0=-74.9\ \text{kJ/mol} \tag{37}$$

4. Fluid dynamics

Hydrodynamics plays an important role in defining the performance of fluidized bed gasifier. Fluidized bed exhibits very complex hydrodynamics due to the nonlinear interactions between fluid and particle and their own individual movement tendencies. Depending on the description of the hydrodynamics, the fluidized bed gasification models may be classified as the two-phase flow model, the Euler–Euler model and the Euler–Lagrange model. Detailed descriptions of each of these models are presented below.

4.1. Two-phase flow model

Two most popular and oldest two-phase flow models are as proposed by Davidson and Harrison [34] and Kunii and Levenspiel [35]. In two-phase flow model, the fluidized bed is divided into two phase e.g. the bubble phase and the emulsion phase (Fig. 4). The bubble phase is assumed to be particle free. The emulsion phase

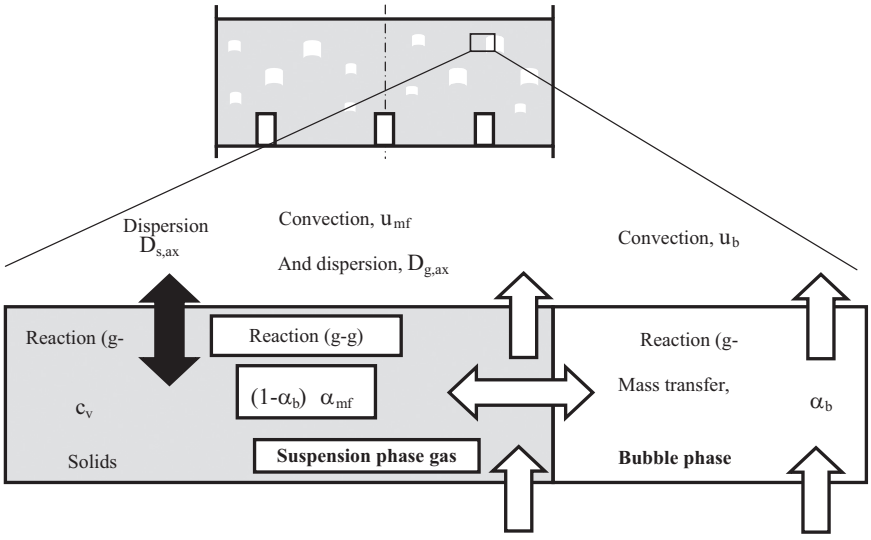

Fig. 4. Division of fluidized bed into bubble and emulsion phases in two-phase flow model.

contains particles and remains in minimum fluidization condition. Gas flows in plug flow in both the bubble and emulsion phase. The solids are evenly distributed and are transported by dispersion only. The heterogeneous gas–solid reactions occur in the emulsion phase only. Homogeneous gas reactions take place in both the bubble and the emulsion phase. The model posses separate mass balance equation for each phase and mass interaction between phases. In two-phase flow model, the momentum equation is not explicitly solved rather the hydrodynamic of the fluidized bed is calculated from correlations. While modeling fluidized bed by using two-fluid model, the gasifier is axially divided into different zones (bottom zone, freeboard and exit zone). The freeboard and the exit zone are generally modeled by comparatively simple mixture model. The two-phase flow concept is used to model the dense bottom zone in fluidized bed systems. Mathematical equations used for such a two-phase flow model following the work of Kruse and Werther [36] and Petersen and Werther [22,37] are given below.

In two-phase flow model, separate mass conservation equations are solved for gas and solid species. Gaseous species are present both in bubble and emulsion phases and hence separate mass conservation equations are solved for gas species in bubble and emulsion phases.

The conservation equation for the gaseous component *i*in the bubble phase is given by

$$\alpha_b \frac{\partial C_{gb,i}}{\partial t} + \frac{\partial (u_b C_{gb,i})}{\partial z} = -K_{be}(C_{gb,i} - C_{ge,i}) + \alpha_b \sum_{j(g-g)} v_{i,j} r_{b,j} \tag{38}$$

The conservation equation for the gaseous component *i* in the emulsion phase is given by

$$(1-\alpha_b)\alpha_{mf}\frac{\partial C_{ge,i}}{\partial t} + (1-\alpha_b)u_{mf}\frac{\partial (C_{ge,i})}{\partial z} - (1-\alpha_b)\alpha_{mf} D_{g,ax}\frac{\partial^2 (C_{ge,i})}{\partial z^2} = K_{be}(C_{gb,i} - C_{ge,i}) + (1-\alpha_b)\alpha_{mf}\sum_{j(g-s)} v_{i,j} r_{emul,j} + c_{v,bz}\sum_{j(g-g)} v_{i,j} r_{emul,j} \tag{39}$$

The particles are present in the emulsion phase only. Hence, the mass balance equation of solid component *i*in the emulsion phase is given by

$$c_v \rho_s \frac{\partial x_{s,i}}{\partial t} - c_v \rho_s D_{s,ax}\frac{\partial^2 (x_{s,i})}{\partial z^2} = \dot{m}'''_{Feed,i} + \dot{m}'''_{Return,i} + c_v M_i \sum_{j(g-s)} v_{i,j} r_{emul,j} \tag{40}$$

where α_b is the void fraction of bubble phase, α_{mf} is the void fraction at minimum fluidization condition, c_v is the solid volume concentration, u_b is the velocity of gas in the bubble phase, u_{mf} is the minimum fluidization velocity, $C_{gb,i}$ is the concentration of gas species i in the bubble phase, $C_{ge,i}$ is the concentration of gas species i in the emulsion phase, $x_{s,i}$ is the mass fraction of solid species i, K_{be} is the mass transfer coefficient between bubble and emulsion phase, $v_{i,j}$ is the stoichiometric coefficient of species i in reaction j, $D_{g,ax}$ is the axial dispersion coefficient of gas phase, $D_{s,ax}$ is the axial dispersion coefficient of solid, $r_{b,j}$ is the reaction rate of reaction $j$in bubble phase, $r_{emul,j}$ is the reaction rate of reaction j in emulsion phase, $\dot{m}'''_{Feed,i}$ is the volumetric mass flow rate at the feeding section, $m'''_{Return,i}$ is the volumetric mass flow rate at the return leg and M_i is the molar mass of species i.

The above mass balance equations are discrelized and numerically solved with appropriate initial and boundary conditions. In two-phase flow model, the fluid dynamic parameters are calculated based on correlations and supplied as input parameters. Several expressions exist to calculate these parameters. A list of hydrodynamic parameters generally used in two-phase flow modeling is given in Table 2. Therefore, the need to solve the momentum equations is avoided and the model becomes comparatively simple. A typical solution procedure for two-phase flow modeling of fluidized bed gasification process is shown in Fig. 5.

Several studies are reported on fluidized bed gasification by using the two-phase flow modeling concept discussed above or in modified form by assuming or estimating several terms. Jiang and Morey [33] studied the fluidized bed biomass gasification by using one dimensional steady-state two-phase flow. The model predicted fuel feed rate, composition of product gas and fuel energy conversion. Model results were compared with experimental date. It was observed that model worked well at higher temperature

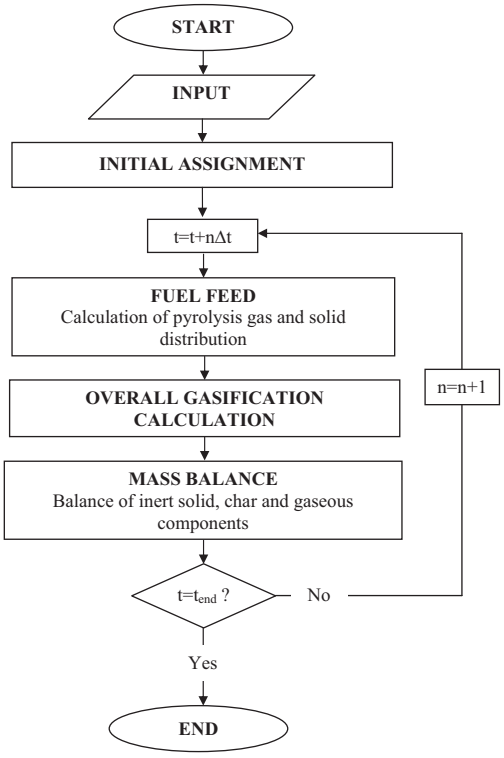

Fig. 5. Flowchart for solution procedure of two-phase flow model.

Table 2
Correlations used for calculating the hydrodynamic parameters in two-phase flow model.

A widely used correlation given by Wen and Yu [38] for calculating $u_{mf}$is given by

$u_{mf} = \frac{\mathrm{Re}_{p,mf}\mu_g}{d_p \rho_g}$, where $\mathrm{Re}_{p,mf} = \sqrt{C_1^2 + C_2 Ar} - C_1$ and $Ar = \frac{d_p \rho_g (\rho_s - \rho_g) g}{\mu_g^2}$

Several values for $C_1$and C_2 are proposed in the literature [39].

The void fraction at minimum fluidization (α_{mf}) can be calculated by solving the equation derived from Ergun equation [79]

$\frac{1.75}{\alpha_{mf}^3 \phi_s}\mathrm{Re}_{p,mf}^2 + \frac{150(1-\alpha_{mf})}{\alpha_{mf}^2 \phi_s^2}\mathrm{Re}_{p,mf} = Ar$

The void fraction of bubble (α_b) can be calculated as

$\alpha_b = 1 - \frac{c_v}{(1-\alpha_{mf})}$

The solid volume concentration c_v can be calculated as

$c_v = (1-\alpha_b)(1-\alpha_{mf})$

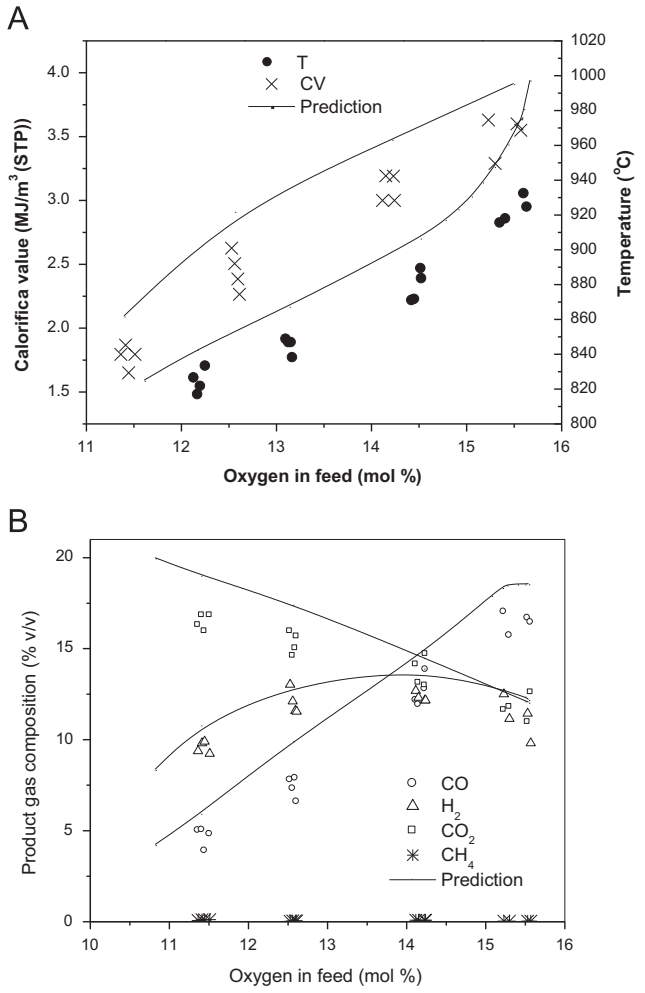

Fig. 6. Effect of oxygen in the feed on (A) bed temperature and calorific value and (B) product gas composition. Steam: 6.8 kg/h; Coal: coke-breeze, 10 kg/h [40].

and for low temperature it was not good. Chatterjee et al. [40] studied the gasification of high ash Indian coal in a lab-scale fluidized bed gasifier by using two-phase flow model. Steam-and air was used as the gasifying agent. The gas composition, temperature, carbon conversion and calorific value of gas with different operating conditions were simulated. The comparison between simulated and experimental results showed similar trend. For example, the simulated and experimental gas composition, calorific value and temperature as a function of oxygen feed rate for coke-breeze and bituminous coal were shown (Fig. 6) and the estimated error between prediction and experiment was within 12%. Yan et al. [41] studied the fluidized bed coal gasification by using two-phase flow model and showed that the change in volume of gas due to reaction resulted in a higher velocity. The suspension phase gas stayed at minimum fluidization, only the bubble phase gas velocity was increased. Thus, a net-flow concept was accounted for which considered the production or reduction of gaseous volume by reaction and it was directed from the suspension phase to the bubble phase. The results showed that the net-flow is significant, in the range 71–87 %, relative to the feed gas rate. Simulation without net-flow deviated significantly from experiment. Jennen et al. [42] studied the gasification of wood in a pilot-scale circulating fluidized bed by using one-dimensional two-phase flow model. The calculated axial profile of the gas composition and the temperature are compared with the experimental data and very good match was found. The difference between the measured and the calculated gas composition was $\pm 1\%$ and maximum deviation of temperature was 5 °C. Hamel and Krumm [43] used the two-phase flow model to simulate four bubbling fluidized bed gasifiers of different scale from atmospheric lab-scale to pressurized commercial-scale. Simulated results of overall carbon conversion, freeboard temperature and the gas species concentration deviated $\pm 10\%$ from experiment. Fiaschi and Michelini [44] used a two-phase flow model to study the biomass gasification kinetics in bubbling fluidized bed gasifier. The model predicted temperature and concentration gradient along the axis. The model result showed largely satisfactory agreement with the experimental result from the literature and the requirement of further validation of the model was identified. Sadaka et al. [45–47] developed a two-phase model for predicting the performance of dual distributor type fluidized bed biomass gasifier. They assumed that the fluidized bed consisted of a dilute phase (jets, bubbles and/or slugs) and an emulsion phase. The emulsion phase was divided into an interstitial gas phase and a solid phase. Model predicted the bed temperature, gas composition, heating value and gas yield. Sensitivity analysis was carried out by varying fluidization velocity, steam flow rate and biomass-to-steam ratio. The model results predicted the experimental data with higher accuracy ($R^2 = 0.88 - 0.98$). Chejne and Hernandez [48] developed a one dimensional two-phase model to simulate the coal gasification in fluidized bed. The model predicted temperature, gas composition, volume fraction, velocity and other fluid dynamic parameters. The model results showed 20% error while compared with the experimental results from the literature. Ross et al. [49] improved the isothermal two-phase flow model by considering the non-isothermal behavior of gases and heat transfer mechanisms and used to study the fluidized-bed coal gasification process. Isothermal and non-isothermal simulations were run for the pilot-scale and commercial-scale gasifier. Gas composition, bed temperature and reaction rate were predicted. The good agreement with experimental results was found for non-isothermal simulation and significant deviation was found for isothermal simulation. Petersen and Werther [22] used two-phase flow models for simulating the gasification of sewage sludge in a pilot-scale circulating fluidized bed gasifier. Initially, a pseudo-two-dimensional model was developed and the gas composition was calculated by selecting the reaction kinetics from the literature. Then the kinetics of pyrolysis and main gasification reactions were determined by comparing the pseudo-two-dimensional model results with the experimental data. Finally, a three-dimensional model [36] was developed with the modified reaction kinetics. Fig. 7 shows the axial gas composition profile for pyrolysis, CO_2 gasification and air-gasification obtained from experiment and pseudo-two-dimensional model with fitting parameters. Good agreement between calculated and measured gas composition was seen after fine tuning the reaction kinetics. Radmanesh et al. [50] used one dimensional isothermal two-phase flow model to study the fluidized bed gasification of biomass. Two different kinetic models for pyrolysis were used and their impact was studied. The effect of equivalence ratio, steam-to-biomass ratio, bed temperature, feed location, and mass transfer between the countercurrent regions on the gas composition was studied. They showed the importance of the pyrolysis step in predicting the final gas composition by comparing the simulated gas composition with experimental data. The pyrolysis model derived at higher heating rates estimated the final gas composition relatively better than the one derived at lower heating rate. The strong influence of pyrolysis step on the overall performance of the fluidized bed biomass gasification was also identified by Kaushal et al. [51] in their two-phase flow modeling study. Pengmei et al. [52] studied the biomass gasification in fluidized bed using two-phase flow model and showed that the trend of changing the gas composition with temperature was in accordance with the experiment. However, the

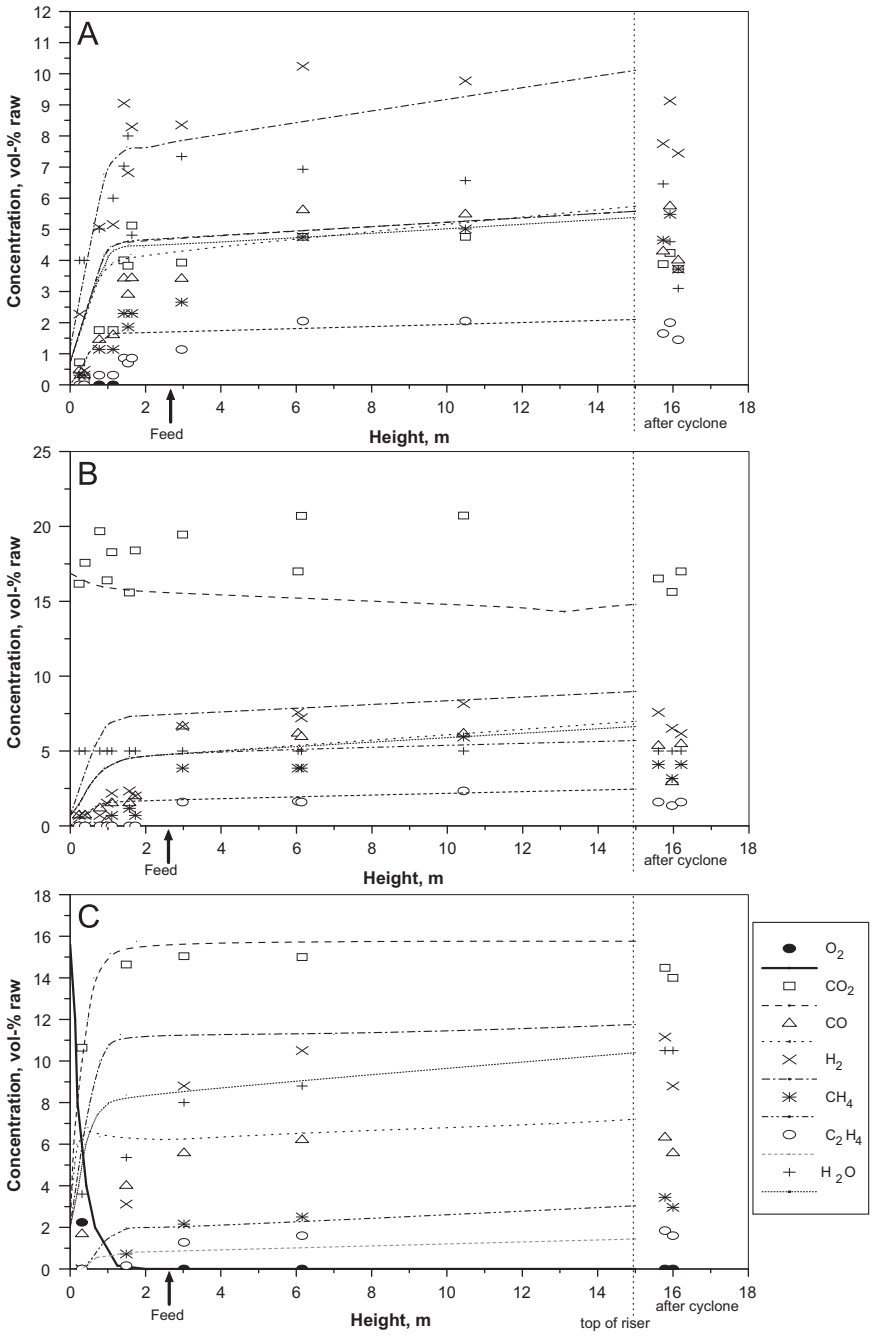

Fig. 7. Axial profile of simulated and measured gas composition in (A) pyrolysis, (B) CO_2 gasification, and (C) air-gasification experiments and modeling results from pseudo-two-dimensional model [36].

gas yield from the simulation was higher that experiment. It was explained that, in simulation, all char particles were assumed to take part in the reaction and no illusion or escape from the bed which resulted more gas yield. Goyal et al. [53] studied the fluidized bed gasification of mixture of coal and petcoke by using two-phase flow model. The effect of various operating parameters such as composition of feed, location of feed point and ash content on the performance of the gasifier were studied. Results showed that the increase in petcoke content in the feed mixture tends to lower the efficiency and carbon conversion but increases the amount of syngas produced and increase in ash content of coal decreases the carbon conversion. The model results also identified that feed point of the solids should be above the point where O_2 in the bed gets exhausted, in order to obtain the maximum carbon conversion and efficiency. Gungor [54] used two-phase flow model to study the fluidized bed biomass gasification process including the tar conversion. Effects of gasification temperature, bed operational velocity, equivalence ratio, biomass particle size and biomass-to-steam ratio on the hydrogen production was studied. The model was capable of predicting concentration distribution of gas species and tar along the height of the gasifier. Simulated hydrogen production was compared with experimental data which showed largely satisfactory agreement but the effect of considering the tar conversion was not shown.

Till date, the two-phase model is the most established model for simulating the fluidized bed gasification process published in the open literature. It is comparatively simple because it does not consider the complex gas–solid dynamics but still maintains the fluid dynamic effect. Therefore, it can provide important information about the fluidized bed gasifier like the transient nature of the

gasifier, distribution of gas species and reacting particles inside the reactor, bubble size and velocity, temperature distribution etc. But, due to the fact that the hydrodynamics is based on some correlations, the applicability of the two-fluid model is restricted to the operating condition on which these correlations are valid. The most common assumption of two-phase flow model is the perfect mixing of solid and plug flow of gas in bubbles and emulsion phases which are sometimes not prevail in the bed. The two-phase flow modeling approach cannot be applied to the freeboard region of the bed, the freeboard is separately modeled. Besides, most of the two-phase flow models are either one dimensional. Therefore, the computational fluid dynamic (CFD) model by coupling the detail fluidized bed hydrodynamics and reaction kinetics may overcome the above disadvantages of two-fluid model and can provides more inside into the fluidized bed gasifier. In CFD models, the hydrodynamics of fluidized bed is based on either the Euler–Euler concept or the Euler–Lagrange concept as discussed below.

4.2. Euler–Euler model

In Euler–Euler model, the gas and the solid phases are treated as interpenetrating continuum present at the same time in the same control volume. The hydrodynamic model uses the conservation of mass and momentum of each phase and represented by respective conservation equations. The interaction between two phases is expressed as additional source terms added to the conservation equations. The conservation equations for mass and momentum are solved for the gas and solid phase separately and are closed with appropriate constitutive relations.

Continuity equation for the gas phase is given by

$$\frac{\partial}{\partial t}(\alpha_g\rho_g)+\nabla.(\alpha_g\rho_g\vec{v}_g)=S_{gs} \tag{41}$$

Continuity equation for the solid phase is given by

$$\frac{\partial}{\partial t}(\alpha_s\rho_s)+\nabla.(\alpha_s\rho_s\vec{v}_s)=S_{gs} \tag{42}$$

where α is the volume fraction, ρ is the density, $\vec{v}$ is the velocity vector and S_{gs} is the mass source term due to chemical reactions. The momentum equation for gas phase is given by the Navier–Stokes equation, modified to include the inter-phase momentum transfer term.

Momentum equation for the gas phase is given by

$$\frac{\partial}{\partial t}(\alpha_g\rho_g\vec{v}_g)+\nabla.(\alpha_g\rho_g\vec{v}_g\vec{v}_g)=-\alpha_g\nabla p+\nabla.\bar{\bar{\tau}}_g+\alpha_g\rho_g\vec{g}+K_{gs}(\vec{v}_s-\vec{v}_g)+S_{gs}\vec{v}_g \tag{43}$$

where p is the hydrodynamics pressure, τ_g is the viscous stress tensor, g is the acceleration due to gravity and K_{gs} is the momentum transfer between gas and solid phases.

The stress tensor of the gas phase can be given as

$$\bar{\bar{\tau}}_g=\alpha_g\mu_g(\nabla\vec{v}_g+\nabla\vec{v}_g^{\,T})-\frac{2}{3}\alpha_g\mu_g.(\nabla.\vec{v}_g)I \tag{44}$$

where μ is the coefficient of viscosity which depends on the thermodynamic state of the fluid for laminar flow and have an added eddy viscosity for turbulent flow.

Since the solid phase is treated as continuous fluid, it has similar properties to a fluid.

Momentum equation for the solid phase is written as

$$\frac{\partial}{\partial t}(\alpha_s\rho_s\vec{v}_s)+\nabla\cdot(\alpha_s\rho_s\vec{v}_s\cdot\vec{v}_s)=-\alpha_s\nabla p-\nabla p_s+\nabla\cdot\bar{\bar{\tau}}_s+\alpha_s\rho_s\vec{g}+K_{gs}(\vec{v}_g-\vec{v}_s)+S_{gs}\vec{v}_s \tag{45}$$

where p_s is the solid pressure and τ_s is the solid phase stress tensor.

The stress tensor for the solid phase is given by

$$\bar{\bar{\tau}}_s=\alpha_s\mu_s\left(\nabla\vec{v}_s+\nabla\vec{v}_s^{\,T}\right)-\alpha_s\left(\lambda_s-\frac{2}{3}\mu_s\right)(\nabla\cdot\vec{v}_s)I \tag{46}$$

where μ_s is the solid shear viscosity and λ_s is the solid bulk viscosity.

The Euler–Euler model became more popular after the development of Kinetic Theory of Granular Flow (KTGF) which is based on the theory of non-uniform dense gases described in the literature [55]. The pioneering paper of Lun et al. [56] applied the kinetic theory of gases to granular flow. Sinclair and Jackson [57] applied the granular flow model to a fully developed gas–solids flow in a pipe. Ding and Gidaspow [58] derived expressions for solids viscosity and pressure of a dense gas–solids flow. Gidaspow [59] extended the Ding and Gidaspow [58] formulation to both dilute and dense phase by considering a non-Maxwellian velocity distribution. Huilin et al. [60] applied KTGF to study the motion of particles in the gas bubbling fluidized bed with the binary mixtures. Louge et al. [61], Pita and Sundareasan [62] and Hrenya and Sinclair [63] incorporated the effects of gas turbulence into their models by modifying single-phase turbulence closures to account for the presence of particle phase. Samuelsberg and Hjertager [64] included the gas turbulence by using LES method and particle–particle interaction using the kinetic theory approach. Nieuwland et al. [65], Balzer et al. [66] and Neri and Gidaspow [67] conducted simulations of gas–solids flow in the circulating fluidized bed using KTGF. Armstrong et al. [68] applied KTGF to study the wall-to-bed heat transfer in a bubbling fluidized bed. Loha et al. [69–71] studied the effect of gas–solid drag model, the solid phase wall boundary condition and coefficient of restitution on the hydrodynamic behavior of a bubbling fluidized bed by using KTGF. Papadikis et al. [72,73] used KTGF to study the effect of drag model and particle size in fluidized bed system. De Wilde and Trujillo [74] applied KTGF to study the catalytic cracking of gas oil in a rotating fluidized bed.

In KTGF, the kinetic energy associated with the particle velocity fluctuations is represented by a pseudo-thermal or granular temperature which is proportional to the mean square of the random motion of particles. A separate partial differential equation is solved for the granular temperature which forms the basis for the turbulence modeling in the solid phase. Then, the solid phase properties like solid viscosity and pressure are described as a function of granular temperature.

The granular temperature equation is represented as

$$\frac{3}{2}\left[\frac{\partial}{\partial t}(\alpha_s\rho_s\Theta_s)+\nabla\cdot(\alpha_s\rho_s\vec{v}_s\Theta_s)\right]=(-p_s\bar{\bar{I}}+\bar{\bar{\tau}}_g):\nabla\vec{v}_s+\nabla\cdot(\kappa_{\Theta s}\nabla\Theta_s)-\gamma_{\Theta s}+\varphi_{gs} \tag{47}$$

where $(-p_s\bar{\bar{I}}+\bar{\bar{\tau}}_g):\nabla\vec{v}_s$ is the generation of energy by solid stress tensor. $\nabla.(\kappa_{\Theta s}\nabla\Theta_s)$ is the diffusion of energy ($\kappa_{\Theta s}$ is the diffusion coefficient). $\gamma_{\Theta s}$ is the collisional dissipation of energy and φ_{gs} is the exchange of fluctuating energy between phase.

In the literature, there is a general agreement on the correlation of solid bulk viscosity and solid pressure [56] which are given below.

$$\lambda_s=\frac{4}{3}\alpha_s\rho_s d_s g_{o,ss}(1+e_{ss})\left(\frac{\Theta_s}{\pi}\right)^{1/2} \tag{48}$$

$$p_s=\alpha_s\rho_s\Theta_s+2\rho_s(1+e_{ss})\alpha_s^2 g_{o,ss}\Theta_s \tag{49}$$

where e_{ss} is the restitution coefficient and $g_{o,ss}$ is the radial distribution function.

For the solids shear viscosity different descriptions are given by different authors and they are listed in Table 3. For example, the equation given by Gidaspow [59] does not account for the inelastic nature of particles in the kinetic contribution of the total stress, as Lun et al. [56] did. The solids shear viscosity of Syamlal et al. [75] neglected the kinetic or streaming contribution, which dominates in dilute-phase flow. Hrenya and Sinclair [63] followed Lun et al. [56]

Table 3
Solid shear viscosity.

Equation	Reference
$\mu_s = \frac{5\sqrt{\pi\Theta}}{96}\rho_s d_s\left[\left(\frac{1}{\eta g_0}+\frac{8\alpha_s}{5}\right)\left(\frac{1+(8/5)\eta(3\eta-2)\alpha_s g_0}{2-\eta}\right)\right]$	Lun et al. [56]
$\mu_s = \frac{4}{5}\alpha_s^2\rho_s d_s g_0(1-e)\sqrt{\frac{\Theta}{\pi}}+\frac{\alpha_s\rho_s d_s\sqrt{\pi\Theta}}{6(3-e)}\left[1+\frac{2}{5}(1+e)(3e-1)\alpha_s g_0\right]$	Syamlal et al. [75]
$\mu_s = \frac{4}{5}\alpha_s^2\rho_s d_s g_0(1+e)\sqrt{\frac{\Theta}{\pi}}+\frac{(5\sqrt{\pi}/48)\rho_s d_s\sqrt{\Theta}}{(1+e)g_0}\left[1+\frac{4}{5}(1+e)\alpha_s g_0\right]^2$	Gidaspow [59]
$\mu_s = \frac{5\sqrt{\pi\Theta}}{96}\rho_s d_s\left[\left(\frac{1}{1+(\lambda_{mfp}/R)}\frac{1}{\eta g_0}+\frac{8\alpha_s}{5}\right)\left(\frac{1+(8/5)\eta(3\eta-2)\alpha_s g_0}{2-\eta}\right)+\frac{768}{25\pi}\eta\alpha_s^2 g_0\right]$	Hrenya and Sinclair [63]

Table 4
Gas–solid drag models.

Equation	Reference
$K_{gs} = \frac{\rho_s\alpha_g g}{u_t\alpha_s^n}$	Richardson and Zaki [76]
$K_{gs} = \frac{3}{4}C_D\frac{\rho_g\alpha_s}{d_s}\left\vert\vec{v}_s-\vec{v}_g\right\vert\alpha_g^{-2.65}$	Wen and Yu [77]
$C_D = \frac{24}{\alpha_g \mathrm{Re}_s}\left[1+0.15(\alpha_g\mathrm{Re}_s)^{0.687}\right]$	
$K_{gs} = \frac{3\alpha_s\alpha_g\rho_g}{4v_{r,s}^2 d_s}C_D\left(\frac{\mathrm{Re}_s}{v_{r,s}}\right)\left\vert\vec{v}_s-\vec{v}_g\right\vert,$	Syamlal-O'Brine [75]
$C_D = \left(0.63+\frac{4.8}{\sqrt{\mathrm{Re}_s/v_{r,s}}}\right)^2,\ \mathrm{Re}_s = \frac{\rho_g d_s\left\vert\vec{v}_s-\vec{v}_g\right\vert}{\mu_l},$	
$v_{r,s} = 0.5\left(A-0.06\mathrm{Re}_s+\sqrt{(0.06\mathrm{Re}_s)^2+0.12(2B-A)+A^2}\right),$	
$A=\alpha_g^{4.14};\quad B=0.8\alpha_g^{1.28}\ \text{for}\ \alpha_g\le 0.85;\quad B=\alpha_g^{2.65}\ \text{for}\ \alpha_g>0.85$	
$K_{gs} = \left[\frac{17.3}{\mathrm{Re}_s}+0.336\right]\frac{\rho_g}{d_s}\left\vert\vec{v}_s-\vec{v}_g\right\vert\alpha_s\alpha_g^{-1.8}$	Gibilaro et al. [82]
$\mathrm{Re}_s = \frac{d_s\alpha_g\left\vert\vec{v}_s-\vec{v}_g\right\vert\rho_g}{2\mu_g}$	
$K_{gs} = \left[\frac{17.3}{\mathrm{Re}_s}+0.336\right]\frac{\rho_g}{d_s}\left\vert\vec{v}_s-\vec{v}_g\right\vert\alpha_s\alpha_g^{-2.8}$	Arastoopour et al. [80]
$\mathrm{Re}_s = \frac{d_s\left\vert\vec{v}_s-\vec{v}_g\right\vert\rho_g}{\mu_g}$	
$K_{gs} = 150\frac{\alpha_s^2\mu_g}{\alpha_g d_s^2}+1.75\frac{\alpha_s\rho_g}{d_s}\left\vert\vec{v}_s-\vec{v}_g\right\vert,\quad \alpha_g<0.8$	Gidaspow [59]
$K_{gs} = \frac{3}{4}C_D\frac{\rho_g\alpha_s}{d_p}\left\vert\vec{v}_s-\vec{v}_g\right\vert\alpha_g^{-2.65},\quad \alpha_g\ge 0.8$	
$C_D = \begin{cases}\frac{24}{\alpha_g\mathrm{Re}_s}\left[1+0.15(\alpha_g\mathrm{Re}_s)^{0.687}\right], & \mathrm{Re}_s<1000\\ 0.44, & \mathrm{Re}_s\ge 1000\end{cases}$	
$\mathrm{Re}_s = \frac{\rho_g\left\vert\vec{v}_s-\vec{v}_g\right\vert d_s}{\mu_g}$	
$K_{gs} = C\left(\frac{17.3}{\mathrm{Re}_s}+0.336\right)\frac{\rho_g\left\vert\vec{v}_s-\vec{v}_g\right\vert}{d_s}\alpha_s\alpha_g^{-1.8}$	McKeen and Pugsley [81]
$\mathrm{Re}_s = \frac{\rho_g d_s\left\vert\vec{v}_s-\vec{v}_g\right\vert\varepsilon_g}{\mu_g}$	
$K_{gs} = 150\frac{\alpha_s^2\mu_g}{\alpha_g d_s^2}+1.75\frac{\alpha_s\rho_g}{d_s}\left\vert\vec{v}_s-\vec{v}_g\right\vert,\quad \alpha_g<0.74$	Yang et al. [83]
$K_{gs} = \frac{3}{4}C_D\frac{\rho_g\alpha_g\alpha_s}{d_s}\left\vert\vec{v}_s-\vec{v}_g\right\vert\omega$	
$-0.5760+\frac{0.0214}{4(\alpha_g-0.7463)^2+0.0044},\quad 0.74\le\alpha_g\le 0.82$	
$-0.0101+\frac{0.0038}{4(\alpha_g-0.7789)^2+0.0040},\quad 0.82\le\alpha_g\le 0.97$	
$-31.8295+32.8295,\quad \alpha_g>0.97$	

approach, but constrained the mean free path of the particle by a dimension characteristic of the actual physical system.

The gas–solid drag model plays an important role in fluidized bed modeling. Different gas–solid drag models are available in the literature and they are listed in Table 4. An earlier drag model was proposed by Richardson and Zaki [76]. Wen and Yu [77] proposed a drag model by extending the work of Richardson and Zaki [76]. The model proposed by Syamlal-O'Brien [78] which was based on the measurement of terminal velocity of solid particle in the fluidized bed. The Gidaspow mode [59] was a combination of Wen and Yu model [77] for solid volume fraction lower than 0.2 and Ergun model [79] for solid volume fraction equal or larger than 0.2. Arastoopour et al. [80] proposed a drag model which gave continuous value over all range of solid volume fraction. McKeen and Pugsley [81] proposed a drag model by introducing a constant scale factor in Gibilaro et al. [82] model to reduce the drag force and taking into account the inter particle cohesive force on particle agglomeration. To investigate the dependence of drag coefficient on structure parameters, Yang et al. [83] adopted a structure-dependent drag model based on the energy minimization multi-scale (EMMS) approach.

The Euler–Euler two-fluid model in combination with KTGF is widely applied for investigating the hydrodynamics of fluidized bed system. But, it is difficult to couple the complicated chemical

reactions with the fluidized bed hydrodynamics due to the complex mechanism of heat transfer and chemical reaction need to be modeled in fluidized bed gasification process. To model the chemical reactions, more careful consideration has to be given on the solution of large numbers of energy and species transport equations and nonlinear source terms of complicated chemical reactions. For modeling the fluidized bed system with chemical reaction by using Euler–Euler model, in addition to the continuity and momentum equation, species conservation equation for each gas species and energy equation for gas and solid phase is required to solve.

The species transport equation is given by

$$\frac{\partial}{\partial t}(\rho_g \alpha_g Y_{g,i}) + \nabla(\rho_g \alpha_g \vec{v}_g Y_{g,i}) = -\nabla \cdot (\alpha_g J_{g,i}) + \alpha_g R_{g,i} + R_{s,i} \quad (50)$$

where $J_{g,i}$, $R_{g,i}$ and $R_{s,i}$ are the diffusion flux of species i in gas phase, the net rate of production of homogeneous species i and the homogeneous reaction rate, respectively.

In species transport equations of gas phase, mass diffusion coefficient are used to calculate the diffusion flux of chemical species in turbulent flow using modified Fick's law

$$J_{g,i} = -\left(\rho_g D_{m,i} + \frac{\mu_t}{\sigma_Y}\right) \nabla \cdot Y_{g,i} \quad (51)$$

where σ_Y is the Schmidt number, which is set as 0.7. The diffusion coefficient of the mixture, $D_{m,i}$ is calculated from the binary mass diffusion coefficient $D_{i,j}$ as follows:

$$D_{m,i} = \frac{1 - X_i}{\sum_{j \neq i} X_j / D_{i,j}} \quad (52)$$

The energy transport equations are solved for the specific enthalpy of gas phase and solid phase, which take the form:

$$\frac{\partial}{\partial t}(\alpha_g \rho_g H_g) + \nabla \cdot (\alpha_g \rho_g \vec{v}_g H_g) = \nabla(k_g T_g) + Q_{gs} + S_{gs} H_s \quad (53)$$

and

$$\frac{\partial}{\partial t}(\alpha_s \rho_s H_s) + \nabla \cdot (\alpha_s \rho_s \vec{v}_s H_s) = \nabla(k_s T_s) + Q_{sg} + S_{sg} H_s \quad (54)$$

where H, k, Q are the specific enthalpy, the gas mixture thermal conductivity and the intensity of heat exchange between the gas and solid phases, respectively. The third term on the right hand side is the heat transfer in that the solid phase changed into gas phase.

The specific enthalpy is defined by

$$H = \sum_{i=1}^{n} Y_i H_i \quad (55)$$

where H_i is the enthalpy for each chemical species in the mixture and considers both, thermal and chemical enthalpy

$$H_i = \int_{T_0}^{T} C_{P,i}\, dT + \Delta H_{f,i} \quad (56)$$

where T_0, $C_{P,i}$ and $\Delta H_{f,i}$ are the reference temperature, the heat capacity at constant pressure for the ith species, and the enthalpy of formation for the ith species in the standard state.

The above conservation equations are solved by using CFD technique to get the gas and solid velocity distribution, volume fraction distribution, gas composition distribution and temperature distribution inside the gasifier and their variation with time. A typical solution procedure for Euler–Euler two-fluid modeling of fluidized bed gasification process using Phase Couple SIMPLE algorithm is shown in Fig. 8.

Very few studies on fluidized bed gasification process using Euler–Euler model are available in the literature. Dou et al. [84] and Dou and Song [85] studied the hydrogen production from steam reforming of glycerol in a lab-scale fluidized bed reactor by using the Euler–Euler model. The simulation was performed for a two-dimensional computational domain. The simulated flow

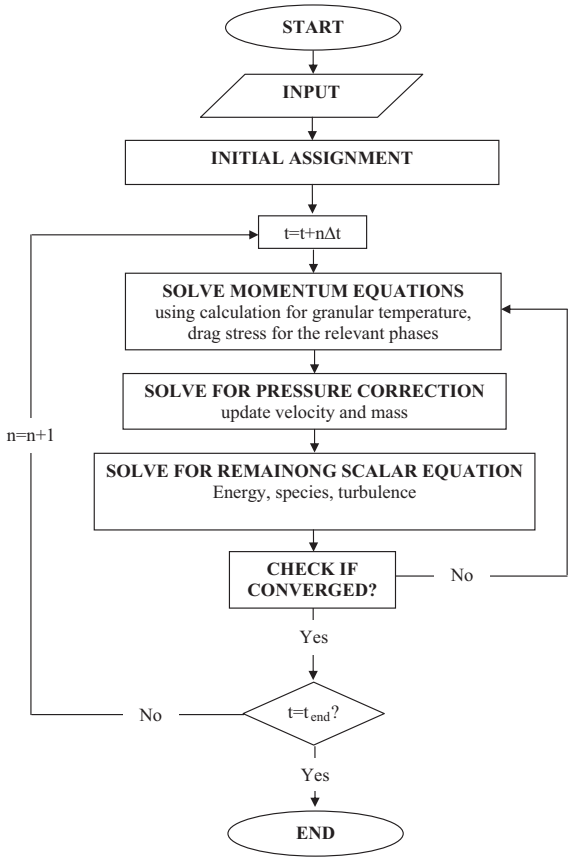

Fig. 8. Flowchart for solution procedure of Euler–Euler CFD model.

Table 5
Comparison between simulated and experimental data for steam reforming of glycerol in fluidized bed reactor [87].

	Experimental data	Simulation
Inlet gas velocity (m/s)	0.5	0.5
Steam to carbon molar ratio (S/C)	2:1	2:1
Catalyst	NiO/Al_2O_3	NiO/Al_2O_3
Temperature (°C)	600	600
H_2 (vol%)	59.1	52.6
CO_2 (vol%)	27.2	33.5
CH_4 (vol%)	5.9	13.9
CO (vol%)	7.8	0.0 (3.5×10^{-15})

distribution exhibited a more heterogeneous core-annuls structure of gas–solid flow which led to back mixing and internal circulation. This flow structure suggested that the bed should be agitated to maintain satisfactory fluidizing conditions. The glycerol conversion and H_2 production variation with inlet gas velocity was studied. The simulated results were also validated with experimental results as shown in Table 5. The difference between simulated and experimental gas composition was less than 8%. But, the model predicted very less (3.5×10^{-15}%) amount of CO. Though, it was mentioned that the error incurred in calculation derived from several sources such as flow and reaction rate model, numerical treatment of initial and boundary conditions and other, but, the specific reason for predicting very less amount of CO composition was not described. Papadikis et al. [86,87] studied the fast pyrolysis of biomass in a lab-scale bubbling fluidized bed reactor by using Euler–Euler model. The Eulerian approach was used to model the bubbling behavior of sand. The discrete description was used for modeling the biomass particle injected inside the reactor and the motion of the particle was computed

using local volume fraction dependent drag laws. 2-D and 3-D simulations were run. It was showed that in the 3-D simulation a bubble was formed close to the feeding point of the reactor and the drag force was quite reduced at the injection time compared with the 2-D case. The simulated hydrodynamic behavior of the bed at different time where biomass particle position was indicated by black spot is shown in Fig. 9. The model gave important information like hydrodynamic of bed with biomass particle position, degradation and evolution of tar with time but no experimental validation was provided. Xue et al. [88] also simulated the fast pyrolysis of biomass in a lab-scale fluidized bed reactor by using Euler–Euler model. Here, gas–particle flow was modeled with a multi-fluid description (gas, sand and biomass). Results indicated that biomass particle size and superficial gas velocity influenced the tar yield and residence time considerably with a fixed bed height. The simulated yields of bio-oil, char and non-condensable gas were compared with the experimental data for pure cellulose and red oak as shown in Table 6. The predicted results showed good quantitative agreement with the experimental data for the yield of each product. But, the model over-predicted the unreacted biomass (residue) particularly for smaller particles. Therefore, it was suggests that a particle size distribution may need to be considered to improve the simulation. Yu et al. [89] simulated the lab-scale bubbling fluidized bed coal gasifier by using Euler–Euler model. Their model was two dimensional and the gasification kinetic was described by 15 species and 11 chemical reactions which include pyrolysis, homogeneous reactions and heterogeneous reactions. The devolatalization and drying was assumed as instantaneous process in the feed zone. Pressure, temperature, velocity, volume fraction of gas composition were predicted. The simulated distribution of gas compositions within the gasifier was plotted for six different operating conditions and two of them are shown here in Fig. 10. It was observed that overall trend of each composition was in consistence with the operating conditions. For example, the concentrations of CO_2 and CO increased along the height of the gasifier, while H_2 and CH_4 go up at first and then drop down to the top of the reactor due to devolatilization and equilibrium of water-gas-shift reactions. This showed that the Euler–Euler model gave more exact prediction which could not be described by two-phase flow model. For validation, the predicted outlet gas compositions for six different operating conditions were compared with the experimental result from the literature as shown in Fig. 11. It was observed that the predicted results agreed well to the experiment with 5% error in CO_2 and N_2 molar fraction and within 20 % error for other results. Wang et al. [90] extended the above simulation in three dimensional geometry to take into account the influences of bed walls and geometry on the flow pattern and other aspects in 3D. Armstrong et al. [91] also simulated the same lab-scale bubbling fluidized bed coal gasifier using Euler–Euler model. They have introduced the limestone calcinations to their model. Their model considered two solid phases one for limestone and other for char which enabled to simulate the segregation of lower density particles (char) to the top of the bed. The hydrodynamic investigation revealed the bubble formation exogenously and endogenously as a result of the reaction kinetics as shown in Fig. 12. A detailed analysis of gasification process was presented from the distribution of gas composition, temperature and reaction rate inside the gasifier. The model results considering inert limestone and limestone calcinations were compared to the experimental data from the literature as shown in Table 7. The model gave reasonably good representation of experimental compositions as a whole. However, unlike experiment, model 1 predicted higher CO than CO_2. They expected that this was due to fact that experimental bed consisted of limestone whereas the model was formed of both char and limestone. However, model 2 gave higher CO_2 compared to model 1 due to the lower initial temperature of the bed. The gas composition did not change significantly by considering limestone calcinations due to slow conversion rate of limestone decomposition. The above simulation was also extended to determine the effects of different bed ratios and over a longer period of time [92].

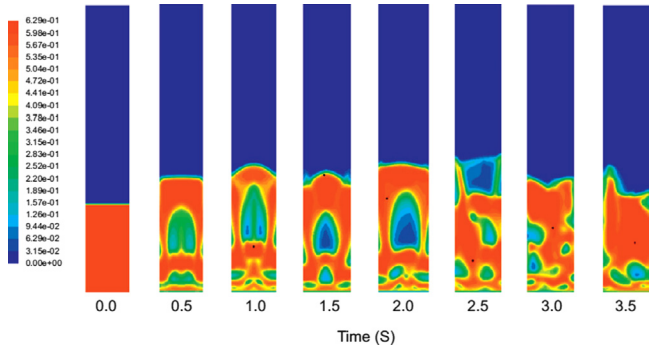

Fig. 9. Fluidized bed hydrodynamics with biomass particle position [89].

The above literature showed that, the Euler–Euler model is an efficient way to study the fluidized bed gasification process where the gas and the solid phases are treated as the interpenetrating continuum and detail momentum equations are solved for both the phases in combination with reaction kinetics to get a detailed insight into the gasifier. In contrast to the two-phase flow model, the Euler–Euler model can simulate the dense bottom bed and freeboard region both simultaneously and the three dimensional flows can be solved. It can provide much more detailed information compared to the two-phase flow model which are very much useful for design and optimization. The Euler–Euler model can predict the bubble formation, bubble rice through the bed, interaction with other bubbles and growth in size and eruption at the upper surface of the bed during fluidized bed gasification process. It can provide the axial and radial variation of gas and solid volume fractions, gas composition, temperature and reaction rates inside the gasifier. In addition to the effect of operating parameters, other effects like position of fuel inlet, gas inlet, outlet, geometry of the

Table 6
Comparison between simulated and experimental product yield for fluidized bed fast pyrolysis of biomass [88].

Method	Bio-oil	Char	Non-considerable gas	Residual	Temperature (°C)
Product yields (wt%) of pure cellulose pyrolysis from experiment and simulation					
Experiment	82.1	2.2	12.4	–	500
Simulation	82.2	3.3	13.9	0.5	493
Product yields (wt%) of a type of red oak pyrolysis from experiment and simulation					
Experiment	71.7 ± 1.4	13.0 ± 1.5	20.5 ± 1.3	–	500
Simulation (d_p=250 μm, 2D)	60.5	12.3	16.2	11.0	497
Simulation (d_p=325 μm, 2D)	62.4	14.1	17.3	6.2	498
Simulation (d_p=325 μm, 2D)	61.5	12.9	16.5	8.7	499
Simulation (d_p=400 μm, 2D)	63.4	15.1	18.1	3.4	499

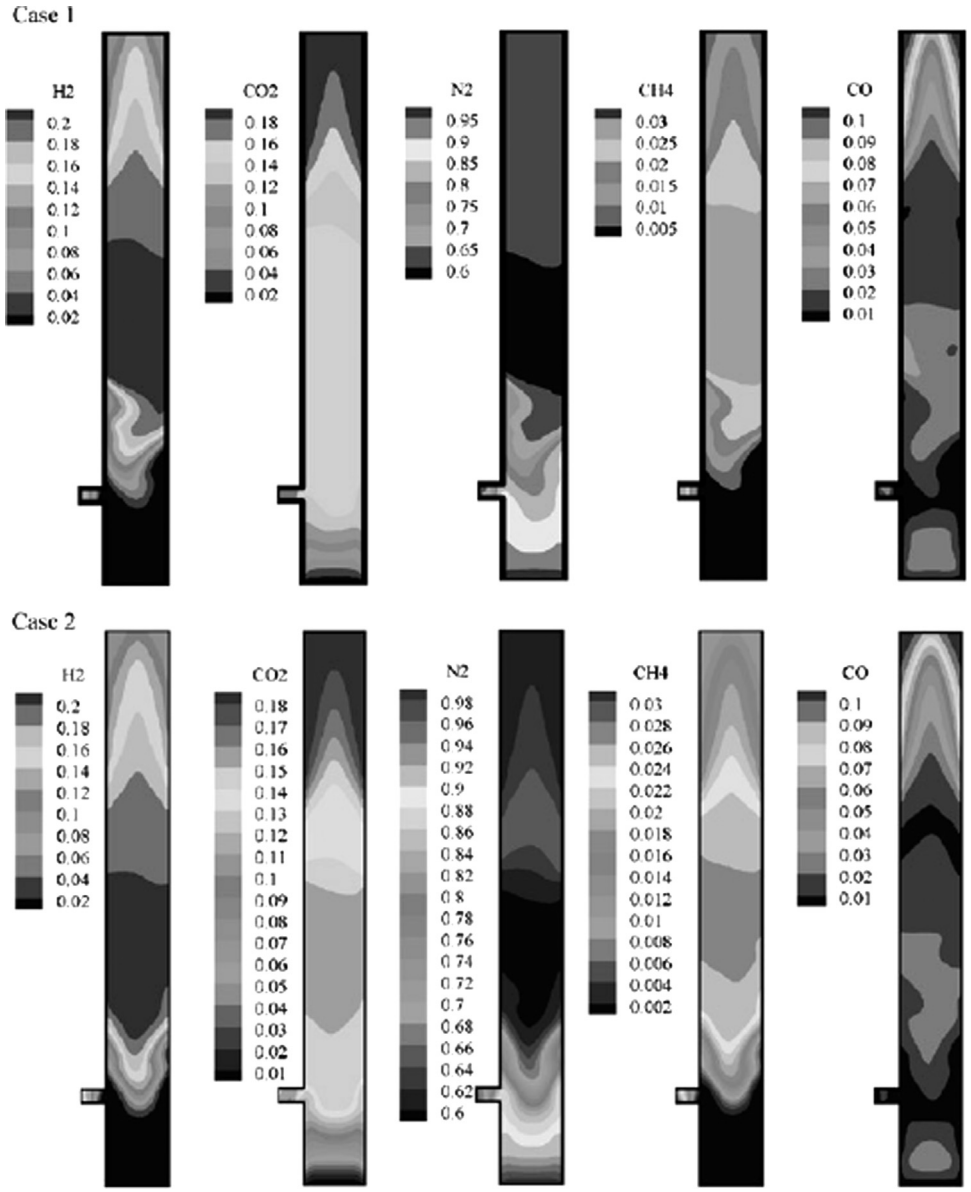

Fig. 10. Concentration distribution of H_2, CO_2, N_2, CH_4 and CO for different operating conditions: Case 1: 8.0 kg/h coal feed, 21.9 kg/h air supply, 4.6 kg/h steam supply, 420 °C air and steam temperature, 855 °C reactor temperature. Case 2: 8.0 kg/h coal feed, 17.0 kg/h air supply, 4.6 kg/h steam supply, 413 °C air and steam temperature, and 812 °C reactor temperature [84].

gasifier, initial bed height etc. can also be studied. In Euler–Euler model, the mixing and segregation between inert bed material and solid fuel particle inside the gasifier can also be studied by taking two different solid phases with different material properties. The Euler–Euler model is computationally less expensive compare to the Euler–Lagrange model because it assumes particles as continuum instead of tracking each and individual particle and hence can be used for modeling large scale fluidized bed gasifier. But, due to the approximation of particle flows as fluid, success of the Euler–Euler model depends on the proper description of particle viscosity and pressure. Besides, to simulate particle size distribution, more than one pseudo-fluid has to be included and all conservation equations are needed to be solved for each pseudofluid which represents one particle size. Therefore, generally Euler–Euler modeling is performed for one or two particle size not for a wide range of particle size distribution. The Euler–Euler model cannot provide information about the residence time of individual reacting particles. Another drawback of Euler–Euler model is that, the particle degradation and shrinkage during gasification process cannot be modeled here. Therefore, to get more particle level information of fluidized bed gasification process, Euler–Lagrange modeling is required.

4.3. Euler–Lagrange model

In Euler–Lagrange model, the gas phase is treated as a continuum and time-averaged Navier–Stoke equations are solved for the gas phase, while the solid phase is solved by tracking each and individual particle in Lagrangian frame of reference. The solid phase exchange mass, momentum and energy with the gas phase. In Euler–Lagrange model, for particle description, discrete element model (DEM)/ discrete particle model (DPM) is commonly applied. In DEM/DPM model, the collision between particles may be either based on soft-sphere approach or hard-sphere approach.

In a hard-sphere approach, the trajectories of the particles are determined by momentum-conserving binary collisions. The interactions between particles are assumed to be pair-wise additive and instantaneous. In the simulation, the collisions are processed one by

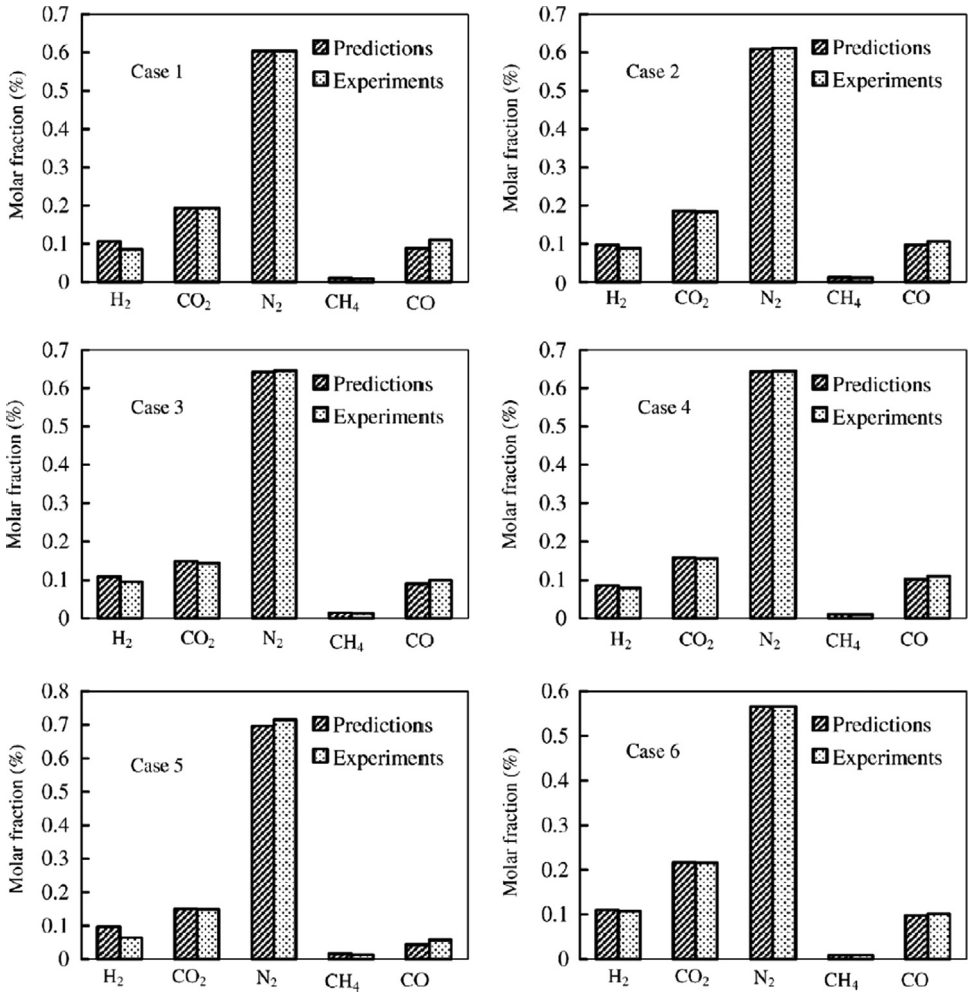

Fig. 11. Comparison between predicted and experimental outlet gas composition for different cases [84].

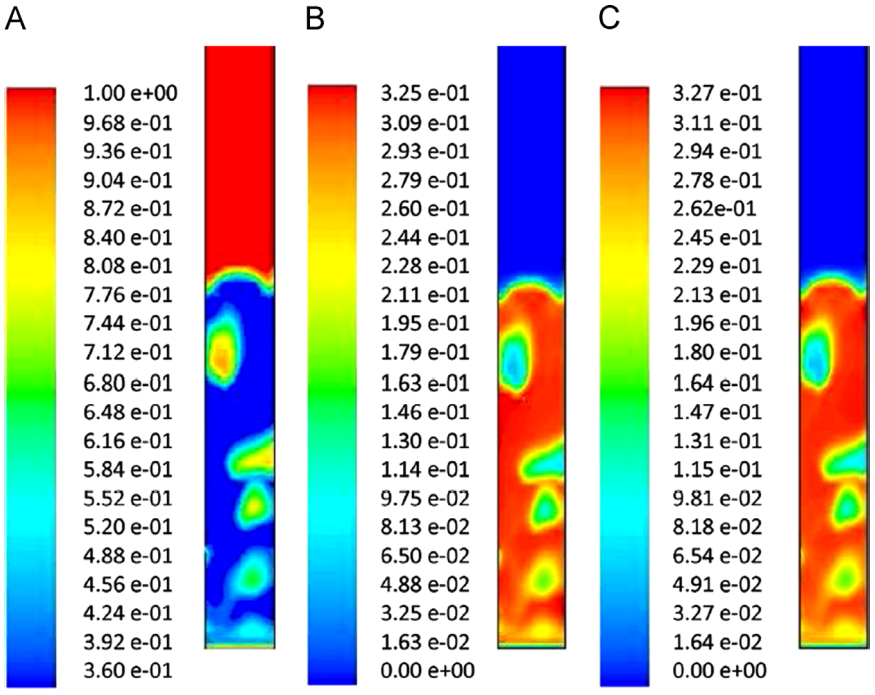

Fig. 12. Volume fraction distribution within the bed for (A) gases, (B) limestone and (C) char [90].

Table 7
Comparison of model results with inert limestone and calcinating limestone and experimental result [91].

	CO	CO_2	H_2	CH_4	N_2	H_2O	Tar
Model 1							
Inert limestone	0.13464	0.09150	0.06226	0.00020	0.54675	0.16428	0.00037
Limestone calcinations	0.13249	0.09279	0.06094	0.00020	0.54671	0.16649	0.00037
Difference	−0.00214	0.00130	−0.00132	0.00000	−0.00003	0.00220	0.00000
Model 2							
Inert llimestone	0.10135	0.09742	0.05230	0.00014	0.52268	0.22584	0.00026
Limestone calcinations	0.10268	0.09818	0.05422	0.00014	0.52379	0.22073	0.00026
Difference	0.00132	0.00076	0.00192	0.00000	0.00111	−0.00511	0.00000
Experiment							
Exp. 1	0.1094	0.1931	0.0853	0.0084	0.6037	N/A	N/A
Exp. 2	0.1059	0.1838	0.0884	0.0107	0.6110	N/A	N/A

one according to the order in which the events occur. For not too dense systems, the hard-sphere models are considerably faster than the soft-sphere models. Occurrence of multiple collisions at the same instant cannot be taken into account in hard sphere model [93]. Campbell and Brennen [94] reported the first hard-sphere simulation used to study granular systems. Since then, the hard-sphere models are applied to study a wide range of complex granular systems. Hoomans et al. [95] used the hard-sphere model in combination with a CFD approach for the gas-phase conservation equations to study gas–solid two fluidized beds. By using this model, they studied the effect of particle–particle interaction on bubble formation and the particle segregation induced by particle size differences and density differences [96]. This model has been further used to study high-pressure fluidization [97,98], circulating fluidized [99], spout-fluid beds [100,101] and particle flows through contractions [102]. Similar simulations are also carried out by many other research groups. For example, Dahl et al. [103] and Dahl and Hrenya [104,105] applied a hard-sphere model to study segregation in continuous size distributions. Ouyang and Li [106,107] developed a slightly different version of this model. Helland et al. [108] developed a DPM in which hard-sphere collisions are assumed, but a time-driven scheme is used to locate the collisional particle pair. Effect of the gas turbulence has also been taken into account in some hard-sphere models [109–114]. At high particle number densities or low coefficient of normal restitution, the collision will lead to a dramatical decrease in kinetic energy. This is the so called inelastic collapse, in which regime the collision frequencies diverge as relative velocities vanish. In that case, the hard sphere method becomes useless. In more complex situations, the particles may interact via short or long-range forces and the trajectories are determined by integrating Newtonian equation motion. The soft-sphere method originally developed by Cundall and Strack [115] was the first granular dynamics simulation technique published in the open literature. Soft-sphere models use a fixed time step and consequently the particles are allowed to overlap slightly. The contact forces are subsequently calculated from the deformation history of the contact using a contact force scheme. The soft-sphere models allow for multiple particle overlap although the net contact force is obtained from the addition of all pair-wise interactions. The soft-sphere models are essentially time driven, where the time step should be carefully chosen in the calculation of the contact forces. The soft-sphere models that can be found in literature mainly differ from each other with respect to the contact force scheme that is used. A review of various popular schemes for repulsive inter-particle forces was presented by Schafer et al. [116]. Walton and Braun [117] developed a force model which uses two different spring constants to model the energy dissipation in the normal and tangential directions respectively. In the force scheme proposed by Langston et al. [118], a continuous potential of an exponential form was used, which contains two unknown parameters: the stiffness of the interaction and an interaction constant. A two-dimensional soft-sphere approach was first applied to gas-fluidized beds by Tsuji et al. [119], where the linear spring/dashpot model similar to the one presented by Cundall and Strack [115] was employed. Kawaguchi et al. [120] extended this model to three dimensions as far as the motion of the particles is concerned. Yu and co-workers [121–123] independently developed a two-dimensional model of a gas-fluidized bed. However, in their simulations a collision detection algorithm that is normally found in hard-sphere simulations was used to determine the first instant of contact precisely. Feng and Yu [124] and Feng et al. [125] applied this model to study segregation processes of a binary mixture. Iwadate and Horio [126] and Mikami et al. [127] developed a model based on Tsuji et al. [119] where they incorporated Van der Waals forces to simulate fluidization of cohesive particles. Further studies of the influence of gas and particle properties for Geldart A particles were performed by Ye et al. [128,129] and Pandit et al. [130]. Kafui et al. [131] developed a DPM based on the theory of contact mechanics, thereby enabling the collision of the particles to be directly specified in terms of material properties such as friction, elasticity, elastoplasticity and auto-adhesion. Limtrakul et al. [132] used the soft-sphere model with mass transfer and chemical reactions to study the decomposition of ozone on catalyst coated particles in a two-dimensional fluidized bed. Kuwagi et al. [133] coupled the soft-sphere model with a model for the description of metallic solid bridging by surface diffusion mechanisms including the effect of surface roughness. Oevermann et al. [134] studied Euler–Lagrange/DEM simulation using soft-sphere method to study wood gasification in bubbling fluidized bed. The soft-sphere DEM model combining with CFD was also used in the literature [135,136] to study the heat transfer in bubbling fluidized beds. Recently, In the following section, only soft-sphere DEM/DPM is discussed because it can in principle handle any situation (dense regimes, multiple contacts) and also additional interaction force. Mathematical equations used for describing the soft-sphere DEM/DPM are given below.

For each particle, the linear momentum equations is given by

$$m_i\frac{dv_i}{dt}=m_i\frac{d^2r_i}{dt^2}=F_{contact,i}+F_{pp,i}+F_{ext,i} \tag{57}$$

where the RHS is the total force on particle, which has three basic contributions:

(i) The total contact force $F_{contact,i}$, which is the sum of individual contact forces exerted by all other particles being in contact with the particle i, which are divided into a normal and a tangential component:

$$F_{contact,i}=F_{contact,N,i}+F_{contact,T,i} \tag{58}$$

(ii) The total external force $F_{ext,i}$:

$$F_{ext,i}=F_{g,i}+F_{d,i}+F_{p,i} \tag{59}$$

where $F_{g,i}$ is the gravitational force, $F_{d,i}$ is the drag force exerted by the surrounding gas phase and $F_{p,i}$ is the pressure force.

(iii) The sum of all other particle–particle forces $F_{pp,a}$, which can include short range cohesive force form the van der Walls interaction between the molecules, as well as long range electrostatic forces.

The angular momentum equation of particle is given by

$$I_i \frac{d\omega_i}{dt} = T_i \tag{60}$$

where I_i is the moment of inertia of particle i and T_i is the torque which depends only on the tangential component of the individual contact forces.

The heat balance for individual particle is given by

$$m_i C_{p,i} \frac{dT_i}{dt} = Q_{gp} + Q_{pp} + Q_{rad} + Q_R \tag{61}$$

where Q_{gp} is the gas–solid convection heat transfer, Q_{pp} is the particle–particle conduction heat transfer, Q_{rad} is the radiation heat transfer and Q_R is the heat transfer due to heterogeneous chemical reactions.

The gas-phase mass and momentum equations are as follows:

$$\frac{\partial}{\partial t}(\alpha_g \rho_g) + \nabla \cdot (\alpha_g \rho_g \vec{v}_g) = S_g \tag{62}$$

$$\frac{\partial}{\partial t}(\alpha_g \rho_g \vec{v}_g) + \nabla \cdot (\alpha_g \rho_g \vec{v}_g \vec{v}_g) = -\alpha_g \nabla p_g + \nabla \cdot (\alpha_g \tau_g) + \alpha_g \rho_g \vec{g} + S_p \tag{63}$$

where α is the volume fraction, ρ is the density, $\vec{v}$ is the velocity vector of gas phase. S_g is the mass source term due to chemical reactions. τ_g is the viscous stress tensor and S_p is the momentum source due to inter-phase interaction. For gas–solid phase in fluidized bed, two-way coupling is required. The S_p is computed by adding up the drag force of the particles located in fluid cell which is given by

$$S_p = \frac{1}{V_{cell}} \sum_{i=1}^{N_p} F_d \tag{64}$$

where V_{cell} is the volume of the fluid cell.

The gas-phase energy equation is given by

$$\frac{\partial}{\partial t}(\alpha_g \rho_g C_{pg} T_g) + \nabla \cdot (\alpha_g \rho_g \vec{v}_g C_{pg} T) = \nabla \cdot (\alpha_g k_g \nabla T_g) + S_{Q,CV} + S_{Q,R} + S_h \tag{65}$$

where T_g is the temperature, C_{pg} is the heat capacity, k_g is the thermal conductivity of the gas phase. $S_{Q,CV}$ is the heat source due to gas–solid convective heat transfer, $S_{Q,R}$ is the heat source due to chemical reactions and S_h is the heat transported by the mass source S_g.

Euler–Lagrange DEM/DPM allows solution for flows with a wide range of particle types, sizes, shapes and velocities. It is able to look at individual discrete particles and their interaction with its local environment. But, due to high collision frequency for volume fractions above 5% and the computational complexity of calculating dense particle–particle interactions, DPM calculations have been limited to on the system having comparatively less numbers of particles [137]. Generally, Euler–Lagrange DEM/DPM is used to study the combustion and gasification of fuel in freeboard area where the particle volume fraction is less. There has been limited study on the simulation of dense gas–solid flow coupling with chemical reactions by using Euler–Lagrange DEM/DPM. Silaen and Wang [138] and Watanabe and Otaka [139] applied Euler–Lagrange DEM/DPM in entrained flow coal gasifier. Gräbner et al. [140] used Euler–Lagrange DEM/DPM at circulating fluidized bed conditions but did not take particle collisions into account. Recently, Bruchmuller et al. [141] studied the thermochemical degradation of biomass inside a lab-scale (38.1 mm diameter and 460 mm height) fast pyrolysis fluidized bed reactor by using Euler–Lagrange DEM/DPM. They have tacked 0.8 million individual discrete sand and biomass particles. This made it possible to look at accurate and detailed multi-scale information (i.e., any desired particle property, trajectory, and particle interaction) over the entire particle life time which revealed that the overall thermochemical degradation process of biomass was influenced by local flow and particle properties. Multiprocessor simulation with high-end computer (2.3 GHz, 192 cores in total distributed on 48 quad cores) was carried out which took 320,000 CPU hours to run 5 s real time.

The Euler–Lagrange DEM/DPM is the most comprehensive model developed till date to study the fluidized bed system. Because, it has the highest potential to realistically reveal thermochemical processes in granular multiphase flow applications. DEM/DPM models are able to accurately predict interparticle and interphase exchange of mass, momentum and energy at the individual particle level without any approximation. Therefore, trajectories, temperature, composition and any other additional particle information are more reliably and more naturally included which are essential to study effects like thermochemical degradation, shrinkage, breakage, segregation, mixing and entrainment. But, the computational time and cost involved in Euler–Lagrange DEM/DPM simulation, restricting the applicability of the model particularly for simulating large-scale fluidized bed reactor which involves more particles and reaction kinetic. Besides, due to its complexity, Euler–Lagrange DEM/DPM simulations are mostly performed in 2-D or quasi-3-D.

Very recently, Euler–Lagrange Computational Particle Fluid Dynamics (CPFD) model is employed for calculating dense particle flow. The CPFD numerical methodology incorporates the multiphase-particle-in-cell (MP-PIC) method [142,143], where the fluid phase is solved by using an Eulerian computational grid and the solids are modeled using Lagrangian computational particles. Here a computational or numerical particle is accounted for via an ensemble of particles displaying the same properties such as chemical composition, size and density. Hence, the number of particles needed to solve can be reduced from billions to millions and this model can be applied to simulate lean as well as dense particle phase flow. Therefore, this model is in between Euler–Euler two-fluid model and Euler–Lagrange DEM/DPM. Andrews and O'Rourke [142] first proposed the MP-PIC method and demonstrated the method with one-dimensional simulations compared to analytical solutions and experimental data. In CPFD three-dimensional forces on each particle is considered which include fluid drag, gravity, static–dynamic friction, particle collision and possibly other forces. Using this method, the particle stress gradient, which is difficult to calculate for each particle in dense flow, is calculated as a gradient to the grid, fully coupled to the other particle and gas acceleration terms and is then interpolated to the discrete particles [144]. In CPFD, cell averaged chemistry is used to calculate the reaction kinetics. Average properties for the particle phase in the chemical rate equations are calculated by interpolating discrete computational particle properties to the grid. The reaction rates are calculated in each grid cell by solving a set of ordinary differential equation. The mathematical equations used for describing the fluid and solid phase in CPFD method are given below.

The volume averaged fluid phase mass and momentum equations are given by

$$\frac{\partial}{\partial t}(\alpha_f \rho_f) + \nabla \cdot (\alpha_f \rho_f \vec{v}_f) = \dot{\rho}_{fs}^{C} \tag{66}$$

$$\frac{\partial}{\partial t}(\alpha_f \rho_f \vec{v}_f) + \nabla \cdot (\alpha_f \rho_f \vec{v}_f \vec{v}_f) = -\nabla p - F + \alpha_f \rho_f g + \nabla \cdot \alpha_f \tau_f \quad (67)$$

where v_f is the fluid velocity and α_f is the fluid volume fraction, ρ_f is the fluid density, p is the fluid pressure, τ_f is the fluid stress tensor and g is the gravitational acceleration. F is the rate of momentum exchange per unit volume between the fluid and the solid phase. The fluid mass production rate per unit volume from solid–fluid chemistry is $\dot{\rho}_{fs}^{C}$.

The constitutive equation for the fluid stress τ_f is given by

$$\tau_{f,ij} = \mu\left(\frac{\partial v_i}{\partial x_j} + \frac{\partial v_j}{\partial x_i}\right) - \frac{2}{3}\mu\delta_{ij}\frac{\partial v_i}{\partial x_j} \quad (68)$$

where μ is the coefficient of viscosity which depends on the thermodynamic state of the fluid for laminar flow and have an added eddy viscosity for turbulent flow based on Smagorinsky turbulence model [145].

The turbulence viscosity is given by

$$\mu_t = C^2 \rho_f \Delta^2 \sqrt{\left(\frac{\partial v_i}{\partial x_j} + \frac{\partial v_j}{\partial x_i}\right)^2} \quad (69)$$

where C is the subgrid scale eddy coefficient and Δ is the length scale.

The fluid phase species equation is given by

$$\frac{\partial}{\partial t}(\alpha_f \rho_f Y_{f,i}) + \nabla \cdot (\alpha_f \rho_f Y_{f,i} \vec{v}_f) = \nabla \cdot (\rho_f \alpha_f D \nabla Y_{f,i}) + \delta m_{i,chem} \quad (70)$$

where $Y_{f,i}$ is the mass fraction of each fluid species and $\delta m_{i,chem}$ is the net production rate of species i due to fluid phase chemical reactions. The coefficient D represents the turbulent mass diffusivity which is related to the viscosity by the Schmidt number ($\mu/\rho_f D = Sc$).

The fluid phase energy equation in terms of the enthalpy is given as

$$\frac{\partial}{\partial t}(\alpha_f \rho_f h_f) + \nabla \cdot (\alpha_f \rho_f h_f \vec{v}_f) = \alpha_f\left(\frac{\partial p}{\partial t} + \vec{v}_f \cdot \nabla p\right) + \Phi + \dot{Q} + S_h + \dot{q}_D + \nabla \cdot (\alpha_f k_f \nabla T_f) \quad (71)$$

where h_f is the fluid phase enthalpy, T_f is the fluid temperature, Φ is the viscous dissipation, $\dot{Q}$ is the energy source per volume, S_h is the energy exchange from the solid face to the fluid phase, and $\dot{q}_D$ is the enthalpy diffusion. The thermal conductivity k_f is the molecular conductivity plus eddy conductivity. For the enthalpy, ideal gas approximation is used, where the enthalpy depends on temperature and the enthalpy for fluid species i is given by

$$h_i = \int_{T_{ref}}^{T} C_{p_i}\, dt + \Delta h_{f,i} \quad (72)$$

where C_p is the specific heat at constant pressure and Δh_f is the heat of formation of the species. The total fluid enthalpy is the mass fraction weighted sum of the fluid species enthalpies.

Prandtl number correlation is given by

$$Pr_t = \frac{C_p \mu_t}{k_t} \quad (73)$$

The enthalpy diffusion term is given by

$$\dot{q}_D = \sum_{i=1}^{N_s} \nabla \cdot (h_i \alpha_f \rho_f D Y_{f,i}) \quad (74)$$

The mixture properties are based on the mass fraction of each gas. The gas phase pressure, temperature and density are related through ideal gas equation. For an ideal gas, the pressure is given by the equation of state as

$$p = \rho_f R T_f \sum_{i}^{N} \frac{Y_{f,i}}{M_i} \quad (75)$$

where, R is the universal gas constant, T_f is gas mixture temperature and M_i is the molecular weight of gas species i.

The dynamics of particle phase is calculated by solving a transport equation for the particle distribution function (PDF) f. It is assumed that f is a function of particle spatial location, particle velocity, particle mass, particle temperature and time. The transport equation for f, which is derived from Boltzmann-BKG approximation model of gas dynamics [146], is given by

$$\frac{\partial f}{\partial t} + \frac{\partial}{\partial x}(fv) + \frac{\partial}{\partial v}(fA) = \frac{f_d - f}{\tau_d} \quad (76)$$

where A is the particle acceleration, f_d is the PDF for the local mass averaged particle velocity, and τ_d is the collision damping time. The particle acceleration A is given by

$$A = \frac{d\vec{v}_s}{dt} = \theta(\vec{v}_f - \vec{v}_s) - \frac{1}{\rho_s}\nabla p + g - \frac{1}{\alpha_s \rho_s}\nabla \tau_s \quad (77)$$

where v_s is the solid velocity, ρ_s is the solid density, α_s is the solid volume fraction, τ_s is the solid normal stress and θ is the momentum transfer coefficient.

The equation for solid movement is given by

$$\frac{d\vec{x}_s}{dt} = \vec{v}_s \quad (78)$$

The energy equation for solid is given by

$$C_v \frac{dT_s}{dt} = \frac{1}{m_s}\frac{k_f Nu_{f,p}}{2r_s} A_s (T_f - T_s) \quad (79)$$

where C_v is the specific heat of the solid material, T_s is the solid temperature, $Nu_{f,p}$ is the Nusselt number of heat transfer in the fluid to the particle.

The particle volume fraction α_s is defined as

$$\alpha_s = \iiint f \frac{m_s}{\rho_s}\, dm_s\, d\vec{v}_s\, dT_s \quad (80)$$

From conservation of volume, the sum of fluid and particle volume fractions equals unity.

$$\alpha_f + \alpha_s = 1. \quad (81)$$

The fluid momentum equation implicitly couples fluid and particles through the inter-phase momentum transfer. The inter-phase momentum transfer at is given by

$$F = -\iiint f\left[m_s\left\{\theta(\vec{v}_f - \vec{v}_s) - \frac{\nabla p}{\rho_s}\right\} + \vec{v}_s \frac{dm_s}{dt}\right] dm_s\, d\vec{v}_s\, dT_s \quad (82)$$

The heat transfer from the solid phase to the gas phase is given by

$$S_h = -\iiint f\left[m_s\left\{\theta(\vec{v}_f - \vec{v}_s)^2 - C_v\frac{dT_s}{dt}\right\} - \frac{dm_s}{dt}\left\{h_s + \frac{1}{2}(\vec{v}_f - \vec{v}_s)^2\right\}\right] dm_s\, d\vec{v}_s\, dT_s \quad (83)$$

where h_s is the particle enthalpy.

5. Numerical solution

In CPFD, the conservation equations are integrated over a control volume. The mixture fluid density, velocity and pressure are coupled by semi-implicit pressure equation derived from the gas mass conservation equation which is applicable to an arbitrary Mach number. The fluid momentum, energy and pressure equations are solved with a conjugated gradient solver. The chemistry of differential equations are calculated using a stiff, sparse ODE solver.

In the MP-PIC scheme, solids properties are mapped to and from the Eulerian grid to get grid properties for the solids. Fluid properties, are in turn, mapped to discrete particle locations. The interpolation operator is the product of interpolation operators in the three orthogonal directions. For a particle located at x_s, where

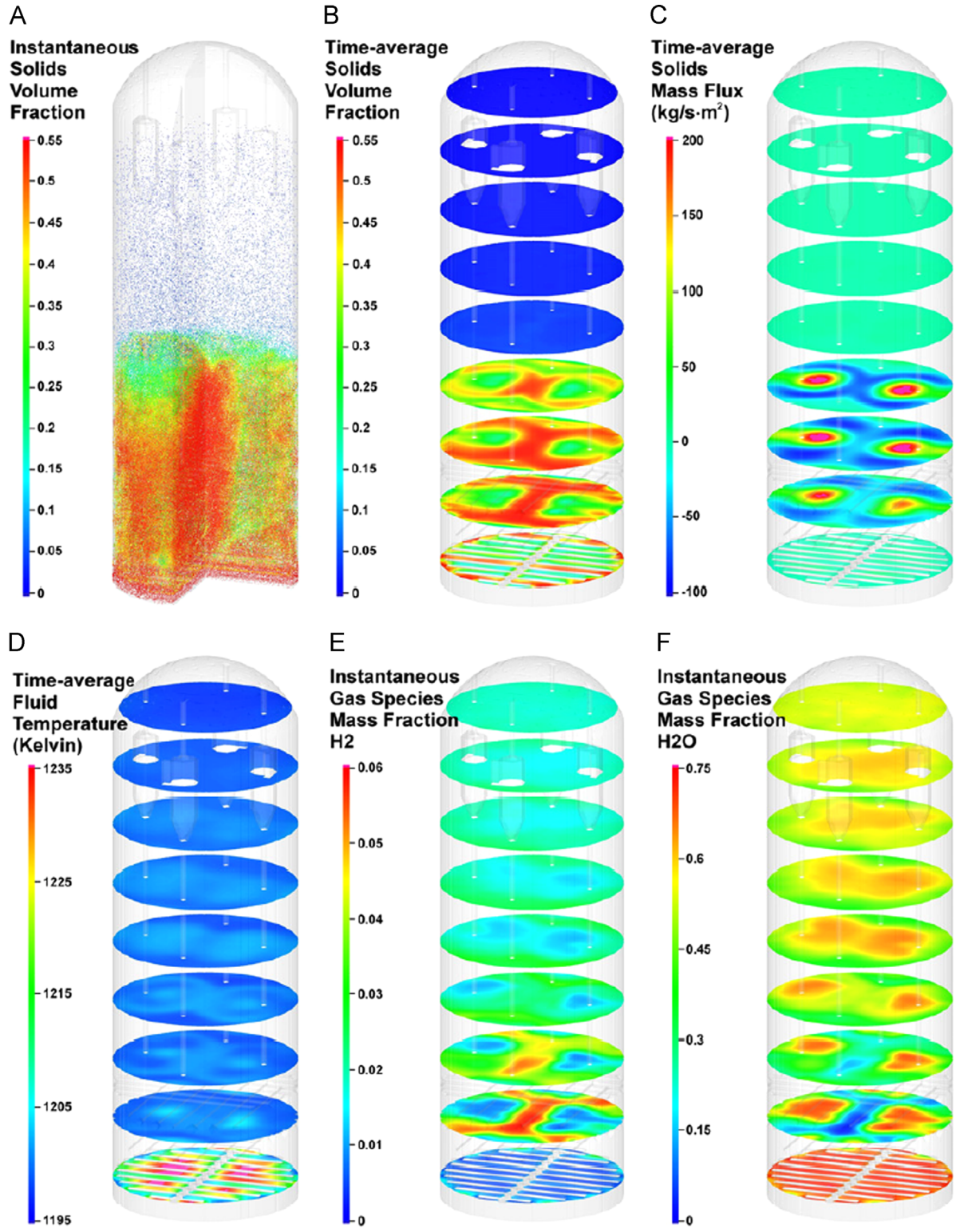

Fig. 13. Gasifier parameters at different axial levels in the reactor [149].

$x_s = (x_s, y_s, z_s)$, the x-directional component of the interpolation operator to grid cell i, is an even function, independent of the y and z coordinates, and has the properties.

$$S_\xi^x(x_s) = \begin{cases} 0, & x_{\xi-1} \geq x_s \geq x_{\xi+1}, \\ 1, & x_s = x_\xi \end{cases} \tag{84}$$

The y and z interpolation operators have a similar form. The particle volume fraction at cell ξ from mapping particle volume to the grid is

$$\alpha_{s\xi} = \frac{1}{V_\xi} \sum_k^{N_s} \frac{m_{sk}}{\rho_{s\xi k}} n_{sk} S_{s\xi k} \tag{85}$$

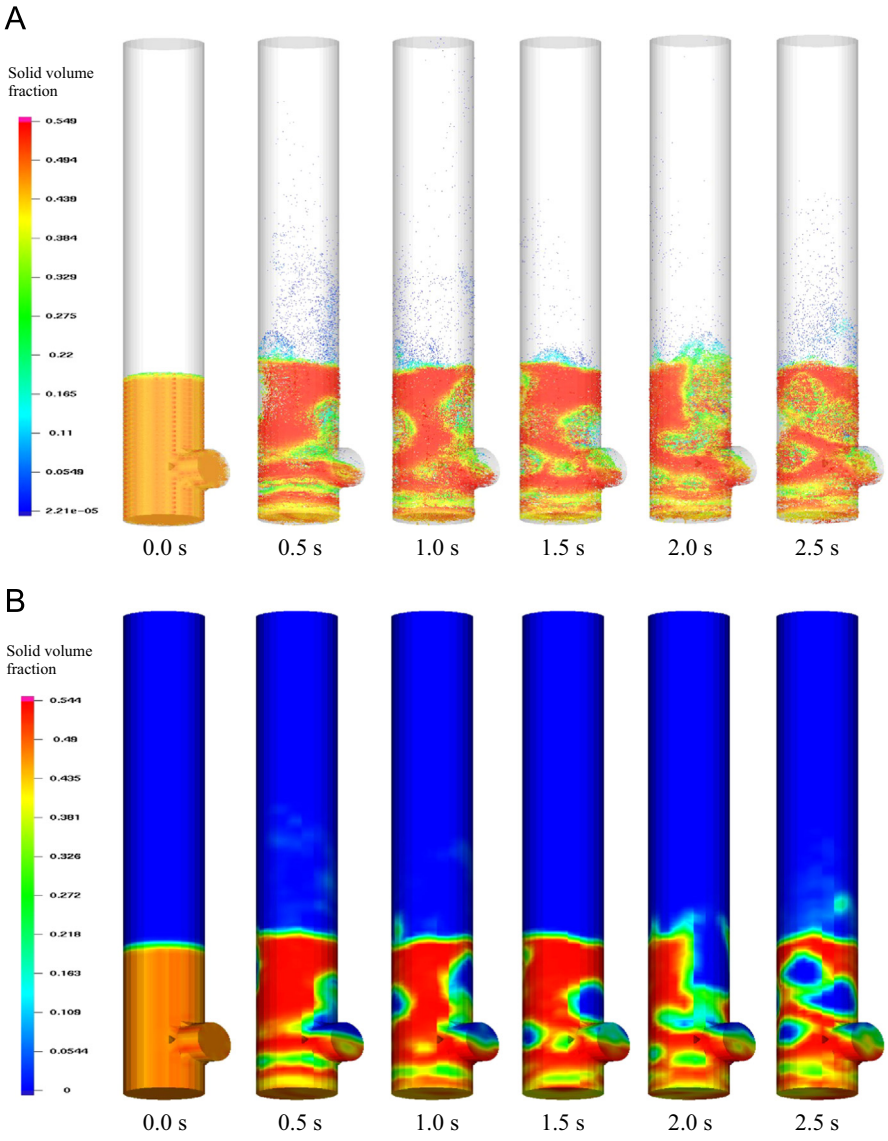

Fig. 14. (A) Discrete solids colored by volume fraction mapped from the grid to particle locations and (B) solids field colored by volume fraction [152].

where V_ξ is the grid volume, n_s is the number of particles in a numerical particle each containing a cloud of particles with identical particle velocity u_s, mass m_s, temperature T_s located at position x_s and the summation is over all numerical particles N_s.

The inter-phase drag coefficient is given by

$$\theta = C_d \frac{3}{8}\frac{\rho_f}{\rho_s}\frac{|v_f - v_s|}{r_s}\alpha_f^{-2.65} \tag{86}$$

where C_d is the drag coefficient. The correlation for C_d based on Wen and Yu [77] is given by

$$C_d = \begin{cases} \frac{24}{\mathrm{Re}}(1+0.15\mathrm{Re}^{0.687}); & \mathrm{Re} < 1000 \\ 0.44, & \mathrm{Re} \geq 1000 \end{cases} \tag{87}$$

and

$$\mathrm{Re} = \frac{2\rho_f |v_f - v_s| r_s}{\mu_f} \tag{88}$$

where r_s is the particle radius as given below.

$$r_s = \left(\frac{3V_s}{4\pi}\right)^{1/3} \tag{89}$$

The particle normal stress is an approximation of collective effects of neighbor particles on a particle. The particle stress is derived from particle volume fraction which is in turn calculated from particle volume mapped to the grid. The particle normal stress model used here is from Harris and Crighton [147] as given below:

$$\tau_s = \frac{P_s \alpha_s^\zeta}{\max[(\alpha_{CP} - \alpha_s),\ \varepsilon(1-\alpha_s)]} \tag{90}$$

where P_s is a positive constant that has the unit of pressure, α_{CP} is the solid volume fraction at close packing limit, ε is a small number on the order of 10^{-7} to remove the singularity and the constant ζ is recommended as $2 \leq \zeta \leq 5$.

The detailed equations and solution algorithm for Euler–Lagrange CPFD model can be found in the literature [143].

Snider and Banerjee [148] applied CPFD numerical to simulate the ozone decomposition in a bubbling fluidized bed. Simulations were run for the full three-dimensional bubbling bed of 0.229 m diameter and 2 m height. The ozone decomposition was described by a single stoichiometric equation with first order reaction rate and isothermal simulation was run. The simulated ozone mass fraction as function of inlet velocity was compared with the analytical solution as well as the experimental result and agreed

well with the both. Snider et al. [149] extended the Eulerian–Lagrangian CPFD methodology to include the heat transfer and chemistry with solid material pyrolysis. The model was used to simulate a large three-dimensional fluidized bed coal gasifier (4.57 m diameter and 13.7 m height) with internal cyclones, internal heaters and as sparger to illustrate the complexity of problem which can be solved by the CPFD method. The gasifier was initially filled with 47,000 kg of solids. The solid was modeled as pure carbon with a particle size distribution. The gasification chemistry was described with five homogeneous and heterogeneous chemical reactions. The gas–solid chemistry consumed the solids and solid shrink from chemistry. The simulation was run for 300 s which took 6 days computational time on a single Intel® Core™ i7 computer. The results from the simulation provided

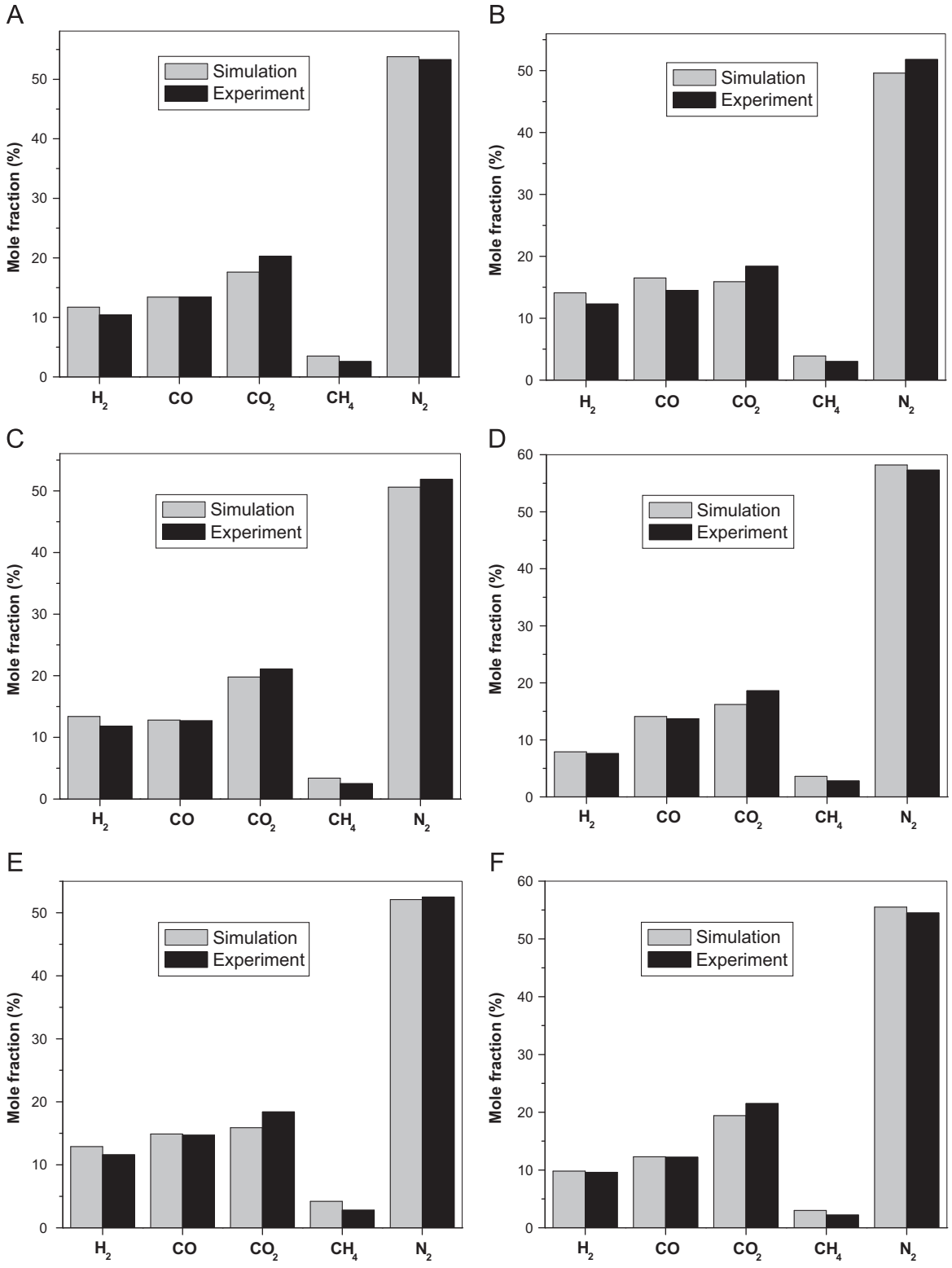

Fig. 15. Comparison between simulated and experimental dry gas compositions: (A) T=800 °C, ER=0.35, S/B=0.5; (B) T=850 °C, ER=0.35, S/B=0.5; (C) T=800 °C, ER=0.35, S/B=0.8; (D) T=800 °C, ER=0.35, S/B=0.2; (E) T=800 °C, ER=0.3, S/B=0.5; and (F) T=800 °C, ER=0.4, S/B=0.5 [152].

insight into the gasifier as discussed below. Fig. 13 shows that the gas–solid flow had regions of high and low volume fraction and large void structures (bubbles) into the bed. The bed surprisingly has a uniform temperature except at the feed-sparger arms where high sensible heat was generated from combustion. There were variations in gas species radially and axially in the bed such as pockets of H_2 above the sparger-distribution-pipe. Abbasi et al. [150] simulated the feeding section of a fast fluidized bed coal gasifier by using CPFD methodology. The solid particles are assumed to remain unchanged in size and the same size distribution was taken for carbon and ash particles. Distribution of particle velocities, particle volume fraction, gas compositions and temperature were obtained. The early sing of chocking in the feeding section was predicted from the simulated particle volume fraction distribution. To compare the CPFD results, a simplified approach, the plug flow reactor (PFR) model was simulated with the same operating conditions. It was found that the time and cross-section average value of temperature and gas compositions simulated by CPFD closely approximated the one for PFR. The CPFD model was also used to study the biomass gasification in three-dimensional lab-scale fluidized bed gasifier [151,152] by considering different particle size for sand and biomass particles. The gas–solid flow pattern, gas composition distribution, parametric variation of gas composition etc. were investigated in details. The bubble formation, development and eruption with time was well captured by complex three dimensional flow structures revealed by the simulation as shown in Fig. 14 [152] whereas only the growth was observed but coalescence and eruption was not identified because of high velocity [151]. It was also observed that the overall dynamics of the bed was strongly influenced by the biomass injection through the side port where the instantaneous devolatization of biomass was assumed. The mode also captured the inherent unsteady nature of the fluidized bed. The comparison of simulated outlet gas composition with experimental data showed reasonable good agreement (Fig. 15). Nevertheless, the CPFD simulation slightly over-predicts H_2, CO and CH_4 generation and under-predicts CO_2. It was concluded that the little discrepancies between experimental and simulated gas compositions may be due to the selection of kinetic parameters based on literature. Xie et al. [153] also simulated the same lab-scale bubbling fluidized bed coal gasifier by using Euler–Lagrange CPFD model which was earlier simulated by using Euler–Euler model [89,91]. In the present model, a particle size distribution was considered instead of a mean particle diameter. The model considered the solid mass consumed or produced in reactions changed the size of particles. The model predicted the gas–solid flow pattern, distribution of gas composition, heterogeneous and homogeneous chemical reaction rates and consumption of carbon mass. Fig. 16 shows the cumulative net consumption of carbon mass with time. It was described that the cumulative consumption of carbon particle mass over 32.5 s was about 0.0098 kg/s, which resulted in the average change of 0.268 μm for solid particle radius. The simulated outlet gas composition also showed good agreement with the experiment with minimum relative error of less than 3%, the maximum relative error of about 30% and the average relative error of less than 15%.

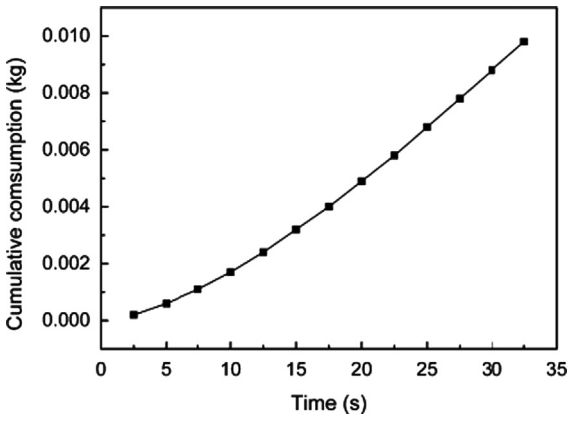

Fig. 16. Cumulative consumption of carbon mass versus time (Q_c=8.0 kg/h, Q_a=28.4 kg/h, Q_s=4.6 kg/h [153]).

The above studies showed that the Euler–Lagrange CPFD model can simulate the fluidized bed gasification process in lab-scale as well as commercial-scale three dimensional gasifier geometry with reasonably less simulation time compared to the Euler–Lagrange DEM/DPM model and also by keeping the Lagrangian description of particles but with the assumption of multiple particles in a cell. It can provide many details inside the gasifier like particle shrinkage due to reaction, residence time of particles, particle size distribution, particle attrition, particle agglomeration etc. which cannot be obtained by Euler–Euler model. It also provides the three dimensional gas–solid flow structure, gas composition distribution, temperature distribution, reaction rate distribution etc. But, the Euler–Lagrange CPFD model cannot provide the information about each and individual particle but can provide the information about each numerical particle (i.e. group of particles having similar property) and hence, it is a tradeoff between the accuracy and the computational cost. Different models used to simulate the fluidized bed gasification process are summarized in Table 8.

6. Conclusion

An updated survey of published mathematical models for fluidized bed gasification process is presented. The present paper describes different modeling approaches starting from the simple models like equilibrium model, two-phase flow model to the very complex Euler–Euler model and Euler–Lagrange models. The basic principle of modeling is discussed in details. Different modeling approaches used by different researchers are reviewed and major results obtained by them are also discussed. The following conclusions may be drawn from the present review.

The equilibrium model is computationally inexpensive. It does not depend on the gasifier type. But, it provides a quick idea about the limiting behavior of a gasification system and hence it is useful for preliminary design of the gasifier. It is observed that the results from the equilibrium model can be improved by modifying it kinetically. While, in kinetic model detailed gasification reaction kinetic is considered with respective rate of reactions. Kinetic models also consider the hydrodynamics of the bed. Depending on the hydrodynamic consideration, the gasification model may be classified as the two-phase flow model, the Euler–Euler model and the Euler–Lagrange model. The two-phase flow modeling is the simplest amongst the rate based or kinetic model because it does not solve any momentum equation for gas or solid. It considers the hydrodynamics of the fluidized bed gasifier which is based on empirical correlations. In Euler–Euler model, both gas and solid are treated as interpenetrating continuum and separate governing equations are solved for each phase. Coupling is achieved through the inter-phase transfer coefficients. It is computationally less expensive compared to the Euler–Lagrange model and also provides reasonably good details about the fluidized bed gasifier. Euler–Lagrange model provides the maximum number of details but computationally more expensive when compute individual particle dynamics (DEM/DPM). Whereas, the Computational Particle Fluid Dynamics (CPFD) model, is a modified Euler–Lagrange model which assumes a numerical particle by combining particles

Table 8
Different models for simulating the fluidized bed gasification process.

Authors	Year	Model type	Key features	Application	Output
Loha et al. [6]	2011	Equilibrium model	Stoichiometric, considered only gaseous species, modified equilibrium constants.	BFB, lab-scale, biomass gasification, steam as gasifying agent.	Parametric variation of gas composition, correlation for product gas.
Loha et al. [7]	2011	Equilibrium model	Stoichiometric, considered gaseous and solid species.	BFB, lab-scale, biomass gasification, steam as gasifying agent.	First law and second law efficiencies, HHV, external energy input, CBP.
Li et al. [10]	2001	Equilibrium model	Non-stoichiometric, RAND algorithm, considered gaseous and solid species, modified with experimental carbon conversion.	CFB, lab-scale, coal gasification, air as gasifying agent.	Parametric variation of gas composition, HHV, carbon conversion, carbon formation boundary, role of moisture
Li et al. [11]	2004	Equilibrium model	Non-stoichiometric, RAND algorithm, considered gaseous and solid species, modified with experimental carbon conversion and methane formation.	CFB, lab-scale, coal gasification, air as gasifying agent.	Parametric variation of gas composition, gas yield, HHV, cold gas efficiency, carbon formation boundary.
Petersen and Werther [22]	2004	Equilibrium model	Stoichiometric, considered only gaseous species.	CFB, pilot-scale, sewage sludge gasification, air as gasifying agent.	Parametric variation of gas composition.
Srinivas et al. [23]	2009	Equilibrium model	Stoichiometric, considered only gaseous species.	CFB, pressurized condition, biomass gasification, air-steam as gasifying agent.	Parametric variation of gas composition, heating value, exergy, efficiency.
Fryda et al. [24]	2008	Equilibrium model	Non-stoichiometric, fixed amount of un-reacted char and CH_4 and tar were introduced based on literature.	FB, lab-scale, biomass gasification, steam as gasifying agent.	Parametric variation of gas composition, efficiency, integrated with SOFC
Schuster et al. [25]	2001	Equilibrium model	Non-stoichiometric, considered gaseous and solid species.	Dual fluidized bed, commercial-scale, biomass gasification, steam as gasifying agent.	Parametric variation of gas composition, heating value, efficiency, carbon formation boundary.
Petersen and Werther [22]	2005	Two-phase flow model	1.5-D, unsteady-state	CFB, pilot-scale, sewage sludge gasification, air as gasifying agent	Axial gas composition variation, comparison with own experimental data, modified the reaction kinetics.
Petersen and Werther [37]	2005	Two-phase flow model	3-D, unsteady-state	CFB, pilot-scale, sewage sludge gasification, air as gasifying agent.	Three dimensional variation of product gas, uneven distribution near feeding point, better mixing with by increasing number of feeding point.
Jiang and Morey [33]	1992	Two-phase flow model	1-D, steady-state, non-isothermal	BFB, lab-scale, biomass gasification, air as gasifying agent.	Fuel feed rate, gas composition, heating value, temperature etc. model agreed well with experiment at higher temperature but failed at lower temperature.
Chatterjee et al. [40]	1995	Two-phase flow model	1-D, steady-state, non-isothermal	BFB, lab-scale, coal gasification, steam and air as gasifying agent.	Variation of gas composition, temperature, calorific value and carbon conversion with oxygen feed and steam feed.
Yan et al. [41]	1998	Two-phase flow model	1-D, steady-state, isothermal, net-flow consideration	BFB, coal gasification.	Bed voidage, reaction rate and gas composition along the height, carbon conversion, significant deviation without considering the net-flow.
Jennen et al. [42]	1999	Two-phase flow model	1-D, non-isothermal, unsteady-state	CFB, pilot-plant, biomass gasification, air as gasifying agent.	Axial gas composition and temperature profile.
Hamel and Krumm [43]	2001	Two-phase flow model	1-D, steady-state, non-isothermal	BFB, lab-scale to commercial-scale. Gasification of brown coal, peat and sawdust. Air, air/steam and O_2/steam as gasifying agent.	Overall carbon conversion, freeboard temperature, gas composition.
Fiaschi and Michelini [44]	2001	Two-phase flow model	1-D, non-isothermal	BFB, biomass gasification, air as gasifying agent.	Gas composition and temperature variation along the axis, optimization with respect to ER, pressure, bed height and gas velocity.
Sadaka et al. [45–47]	2002	Two-phase flow model	1-D, unsteady-state, non-isothermal	Dual distributor type FB, lab-scale, Biomass gasification, Air-steam as gasifying agent.	Gas composition, bed temperature, heating value, gas production rate.
Chejne and Hernandez [48]	2002	Two-phase flow model	1-D, steady-state, non-isothermal.	BFB, lab-scale coal gasification.	Temperature, gas composition, volume fraction, velocity and other fluid dynamic parameters. Strong influence of feed point position was observed in the result.
Ross et al. [49]	2005	Two-phase flow model	1-D, steady-state, non-isothermal.	BFB, commercial-scale and pilot-scale, coal gasification, air-steam as gasifying agent.	Gas composition, temperature and reaction rate along the height, overall carbon conversion.
Radmanesh et al. [50]	2006	Two-phase flow model	1-D, steady-state, Isothermal	BFB, biomass gasification. air-steam as gasifying agent	Gas composition variation with T, ER, S/B, feed location and mass transfer between counter current region.
Kaushal et al. [51]	2010	Two-phase flow model	1-D, steady-state, non-isothermal	BFB, biomass gasification	Temperature, solid hold ups and gas concentration variation along the reactor's major axis.

Table 8 (*continued*)

Authors	Year	Model type	Key features	Application	Output
Pengmei et al. [52]	2008	Two-phase flow model	1-D, steady-state, Isothermal	FB, biomass gasification, air-steam as gasifying agent	Gas composition, gas yield
Goyal et al. [53]	2010	Two-phase flow model	1-D, non-isothermal	BFB, gasification of coal and petcoke mixture	Effect of composition and location of feed point and ash content on the performance, Increase in petcoke content tends to lower the efficiency and carbon conversion but increases the amount of syngas produced, increase in ash content of coal decreases the carbon conversion.
Gungor [54]	2011	Two-phase flow model	1-D, steady-state, isothermal	FB, biomass gasification, air-steam as gasifying agent.	Hydrogen production variation with T, ER, S/B, velocity and particle size.
Dou et al. [84]	2008	Euler–Euler model	2-D, single solid phase and single particle size, unsteady-state, non-isothermal.	BFB, lab-scale, steam reforming of glycerol.	Gas–solid flow pattern, glycerol consumption, hydrogen and other gas production.
Dou and Song [85]	2010	Euler–Euler model	2-D, single solid phase and single particle size, unsteady-state, non-isothermal.	BFB, lab-scale, steam reforming of glycerol.	Gas–solid flow pattern, glycerol consumption, hydrogen and other gas production, detailed analysis of relationship between hydrodynamics and hydrogen production.
Papadikis et al. [86,87]	2008 & 2009	Euler–Euler model	2-D and 3-D, Eulerian description of gas and sand particle, Lagrangian description of single biomass particle.	BFB, Lab-scale, Fast pyrolysis	Gas–solid flow pattern with biomass particle position, gas composition and temperature distribution, tar evolution
Xue et al. [88]	2012	Euler–Euler model	2-D and 3-D simulation, two solid phases for sand and biomass, unsteady-state, isothermal.	BFB, lab-scale, biomass fast pyrolysis	Influence of operating conditions on the conversion process and product yield, model over-predicted the un-reacted biomass elutriation for smaller particles.
Yu et al. [89]	2007	Euler–Euler model	2-D, k–ϵ turbulence model for gas phase, Single solid and single particle size, unsteady-state, non-isothermal.	BFB, lab-scale, coal gasification, air-steam as gasifying agent.	Gas–solid flow pattern, gas composition distribution, reaction rate distribution.
Wang et al. [90]	2009	Euler–Euler model	3-D, k–ϵ turbulence model for gas phase, Single solid phase and single particle size, unsteady-state, non-isothermal.	BFB, lab-scale, coal gasification, air-steam as gasifying agent.	Flow pattern, gas velocity, particle velocity, gas composition distribution, reaction rate distribution.
Armstrong et al. [91]	2011	Euler–Euler model	2-D, separate solid phase for coal, limestone and char. Single particle size for each solid phase, unsteady-state, non-isothermal.	BFB, lab-scale, coal gasification, air-steam as gasifying agent.	Gas–solid flow pattern, distribution of gas composition, reaction rate and temperature. Impact of limestone calcinations on gaseous composition.
Armstrong et al. [92]	2011	Euler–Euler model	2-D, two different devolatilization model, separate solid phase for coal, limestone and char. single particle size for each solid phase, unsteady-state, non-isothermal. extended simulation time (400 s).	BFB, lab-scale, coal gasification, air-steam as gasifying agent.	Gas–solid flow pattern, gas composition variation with bed material composition, bed height, temperature of bed and inclusion of heat transfer coefficient.
Silaen and Wang [138]	2010	Euler–Lagrange DEM/DPM	3-D, four different devolatization models are employed	Entrained flow gasifier, coal gasification, oxygen blown.	Gas composition, temperature, efficiency, effect of different devolatization model.
Watanabe and Otaka [139]	2006	Euler–Lagrange DEM/DPM	2-D, 2 t/day	Entrained flow gasifier, coal gasification.	Influence of the air ratio on carbon conversion efficiency, amount of product char, heating value, and cold gas efficiency, temperature and product gas composition distribution.
Gräbner et al. [140]	2007	Euler–Lagrange DEM/DPM	4800 t/day, high pressure (33 bar).	Winkler gasifier, coal gasification, steam/oxygen as gasifying agent.	Flow pattern, turbulence, product gas composition, temperature and radial heat transfer.
Bruchmuller et al [141]	2012	Euler–Lagrange DEM/DPM	3-D, 0.8 million individual sand and biomass particle.	BFB, lab-scale, biomass fast pyrolysis.	Gas–solid flow pattern, particle degradation, particle entrainment, gas composition distribution.
Snider and Banerjee [148]	2010	Euler–Lagrange CPFD	3-D, constant particle size, only single reaction, unsteady-state.	BFB, lab-scale, ozone decomposition.	Particle volume fraction distribution, ozone mass fraction distribution, variation with velocity.
Snider et al. [149]	2011	Euler–Lagrange CPFD	3-D, 47,000 kg of particle initially, particle size distribution, particle shrinkage from chemistry, unsteady-state, non-isothermal.	Internal CFB, commercial-scale example gasifier, complex geometry with internal cyclones, coal gasification, air-steam as gasifying agent.	Particle volume fraction, gas composition, temperature and reaction rate distribution.
Abbasi et al. [150]	2011	Euler–Lagrange CPFD	2-D, same particle size distribution for coal and ash particle, size does not change due to reaction, unsteady-state, non-isothermal.	Feeding section of a CFB, lab-scale, coal gasification, air-steam as gasifying agent.	Particle volume fraction, and size distribution, fluid velocity, temperature and pressure drop distribution, gas composition distribution.
Xie et al. [151]	2012	Euler–Lagrange CPFD	3-D, different particle species for carbon, ash and sand particle, unsteady-state, isothermal.	BFB, lab-scale, biomass gasification, air-steam as gasifying agent.	Bubble growth was captured but collision and eruption were not visible, gas composition variation with T, S/B, ER. Gas composition distribution.
Loha et al. [152]	2014	Euler–Lagrange CPFD	3-D, different particle species for carbon, ash and sand particle, particle size distribution, unsteady-state, isothermal.	BFB, lab-scale, biomass gasification, steam as gasifying agent.	Bubble formation, development and eruption with time and interaction with, influence of biomass injection through side port, gas composition variation with T, S/B, ER and time.
Xie et al. [153]	2013	Euler–Lagrange CPFD	3-D, different particle species for carbon, ash and sand particle, particle size distribution, particle size changes due to reaction, unsteady-state, non-isothermal.	BFB, lab-scale, coal gasification, air-steam as gasifying agent.	Bubble formation, development and eruption with time, distribution of gas composition, temperature and reaction rate, carbon consumption with time.

of same properties, can simulate large-scale fluidized bed gasifier with comparatively less time. But, the information about each individual particle cannot be provided by the Euler–Lagrange CPFD model.

From the present survey, it is observed that almost in all fluidized bed gasification models only the outlet gas compositions are compared with experiment. There are few measurements available for comparison with detailed model results. Therefore, effort is still required to validate the truly comprehensive fluidized bed models.

Acknowledgment

The authors express their sincere gratitude to The Director, CSIR-CMERI, Durgapur, India for his continuous support and encouragement. The authors are also grateful for the support from EU FP7 iComFluid project (Grant No. 312261).

References

[1] Basu P. Combustion and gasification in fluidized bed. Taylor and Francis Group: CRC Press; 2006.
[2] Buragohain B, Mahanta P, Moholkar VS. Biomass gasification for decentralized power generation: the Indian perspective. Renew Sustain Energy Rev 2010;14:73–92.
[3] Gomez-Barea A, Leckner B. Modeling of biomass gasification in fluidized bed. Prog Energy Combust Sci 2010;36:444–509.
[4] Singh RI, Brink A, Hupa M. CFD modeling to study fluidized bed combustion and gasification. Appl Therm Eng 2013;52:585–614.
[5] Smith RW, Missen WR. Chemical reaction equilibrium analysis: theory and algorithms. New York: Wiley Interscience; 1982.
[6] Loha C, Chatterjee PK, Chattopadhyay H. Performance of fluidized bed steam gasification of biomass—modeling and experiment. Energy Convers Manag 2011;52:1583–8.
[7] Loha C, Chattopadhyay H, Chatterjee PK. Thermodynamic analysis of hydrogen rich synthetic gas generation from fluidized bed gasification of rice husk. Energy 2011;36:4063–71.
[8] JANAF thermochemical tables, 3rd ed., Part 1+2. New York; 1986.
[9] Probstein RF, Hicks RE. Synthetic fuel. New York: McGraw-Hill; 1982.
[10] Li X, Grace JR, Watkinson AP, Lim CJ, Ergudenler A. Equilibrium modeling of gasification: a free energy minimization approach and its application to a circulating fluidized bed coal gasifier. Fuel 2001;80:195–207.
[11] Li X, Grace JR, Lim CJ, Watkinson AP, Chen HP, Kim JR. Biomass gasification in a circulating fluidized bed. Biomass Bioenergy 2004;26:171–93.
[12] White WB, Johnson SM, Dantzig GB. Chemical equilibrium in complex mixtures. J Chem Phys 1958;28:751–5.
[13] Zeleznik FJ. Calculation of complex chemical equilibria. Ind Eng Chem 1968;60:27–57.
[14] Smith RW, Missen WR. Chemical reaction equilibrium analysis: theory and algorithms. New York: Wiley Interscience; 1982.
[15] Zainal ZA, Ali R, Lean CH, Seetharamu KN. Prediction of performance of downdraft gasifier using equilibrium modeling for different biomass material. Energy Convers Manag 2001;42:1499–515.
[16] Rao MS, Singh SP, Sodha MS, Dubey AK, Shyam M. Stoichiometric, mass, energy and exergy balance analysis of countercurrent fixed-bed gasification of post-consumer residues. Biomass Bioenergy 2004;27:155–71.
[17] Prins MJ, Ptasinski KJ, Janssen FJJG. Thermodynamics of gas–char reactions: first and second law analysis. Chem Eng Sci 2003;58:1003–11.
[18] Prins MJ, Ptasinski KJ, Janssen FJJG. From coal to biomass gasification: comparison of thermodynamic efficiency. Energy 2007;32:1248–59.
[19] Jarungthammachote S, Dutta A. Thermodynamic equilibrium model and second law analysis of a downdraft gasifier. Energy 2007;32:1660–9.
[20] Pellegrini LF, de Oliveira S. Exergy analysis of sugarcane bagasse gasification. Energy 2007;32:314–27.
[21] Abuadala A, Dincer I, Naterer GF. Exergy analysis of hydrogen production from biomass gasification. Int J Hydrogen Energy 2010;35:4981–90.
[22] Petersen I, Werther J. Experimental investigation and modeling of gasification of sewage sludge in the circulating fluidized bed. Chem Eng Process 2005;44:717–36.
[23] Srinivas T, Gupta AVSSKS, Reddy BV. Thermodynamic equilibrium model and exergy analysis of a biomass gasifier. ASME J Energy Resour Technol 2009;131:031801-1–7.
[24] Fryda L, Panopoulos KD, Karl J, Kakaras E. Exergetic analysis of solid oxide fuel cell and biomass gasification integration with heat pipes. Energy 2008;33:292–9.
[25] Schuster G, Loffler G, Weigl K, Hofbauer H. Biomass steam gasification—an extensive parametric modelling study. Bioresour Technol 2001;77:71–9.
[26] Badzioch S, Hawksley PGW. Kinetics of thermal decomposition of pulverized coal particles. Ind Eng Chem Process Des Dev 1970;9:521–30.
[27] Kobayashi H. Devolatilization of pulverized coal at high temperatures. (Ph.D. thesis). Cambridge, MA: Department of Mechanical Engineering, Massachusetts Institute of Technology; 1976.
[28] Nunn TR, Howard JB, Longwell JP, Peters WA. Product compositions and kinetics in the rapid pyrolysis of sweet gum hardwood. Ind Eng Chem Proc Des Dev 1985;24:836–44.
[29] Boroson ML, Howard JB, Longwell JP, Peters WA. Product yields and kinetics from the vapor phase cracking of wood pyrolysis tars. AIChE J 1989;35:120–8.
[30] Jand N, Foscolo PU. Decomposition of wood particles in fluidized beds. Ind Eng Chem Res 2005;44:5079–89.
[31] Niksa S. Flashchain theory for rapid coal devolatilization kinetics. 2: impact of operating conditions. Energy Fuels 1991;5:665–73.
[32] Jiang H, Morey RV. Pyrolysis of corncob at fluidization. Biomass Bioenergy 1992;3:81.
[33] Jiang H, Morey RV. A numerical of a fluidized bed biomass gasifier. Biomass Bioenergy 1992;3:431–47.
[34] Davidson JF, Harrison D. Fluidised particles. Cambridge: Cambridge University Press; 1963.
[35] Kunii D, Levenspiel O. Fluidization Engineering. New York: John Wiley; 1969.
[36] Kruse M, Werther J. 2D gas and solids flow prediction in circulating fluidized beds based on suction probe and pressure profile measurements. Chem Eng Process 1995;34:185–203.
[37] Petersen I, Werther J. Three dimensional modeling of circulating fluidized bed gasifier for sewage sludge. Chem Eng Sci 2005;60:4469–84.
[38] Wen CY, Yu YH. A generalized method for predicting the minimum fluidization velocity. AIChE J 1966;12:610–2.
[39] Grace JR. Contacting modes and behaviour classification of gas–solid and other two-phase suspensions. Can J Chem Eng 1986;64:353–63.
[40] Chatterjee PK, Datta AB, Kundu KM. Fluidized bed gasification of coal. Can J Chem Eng 1995;73:204–10.
[41] Yan HM, Heidenreich C, Zhang DK. Mathematical modelling of a bubbling fluidised-bed coal gasifier and the significance of 'net flow'. Fuel 1998;77:1067–79.
[42] Jennen T, Hiller R, Koneke D, Weinspach PM. Modeling of gasification of wood in a circulating fluidized bed. Chem Eng Technol 1999;22:822–6.
[43] Hamel S, Krumm W. mathematical modeling and simulation of bubbling fluidized bed gasifiers. Powder Technol 2001;120:105–12.
[44] Fiaschi D, Michelini M. A two-phase one-dimensional biomass gasification kinetics model. Biomass Bioenergy 2001;21:121–32.
[45] Sadaka SS, Ghaly AE, Sabbah MA. Two phase biomass air–steam gasi_cation model for fluidized bed reactors: Part I—model development. Biomass Bioenergy 2002;22:439–62.
[46] Sadaka SS, Ghaly AE, Sabbah MA. Two phase biomass air-steam gasi_cation model for fluidized bed reactors: Part II—model sensitivity. Biomass Bioenergy 2002;22:463–77.
[47] Sadaka SS, Ghaly AE, Sabbah MA. Two phase biomass air–steam gasi_cation model for fluidized bed reactors: Part III—model validation. Biomass Bioenergy 2002;22:479–87.
[48] Chejne F, Hernandez JP. Modeling and simulation of coal gasification process in fluidized bed. Fuel 2002;81:1687–702.
[49] Ross DP, Yan HM, Zhong Z, Zhang DK. A non-isothermal model of a bubbling fluidized-bed coal gasifier. Fuel 2005;84:1469–81.
[50] Radmanesh R, Chaouki J, Guy C. Biomass gasification in a bubbling fluidized bed reactor: experiments and modeling. AIChE J 2006;52:4258–72.
[51] Kaushal P, Abedi J, Mahinpey N. A comprehensive mathematical model for biomass gasification in a bubbling fluidized bed reactor. Fuel 2010:3650–61.
[52] Pengmei L, Xiaoying K, Chuangzhi W, Zhenhong Y, Longlong M, Jie C. Modeling and simulation of biomass air–steam gasification in a fluidized bed. Front Chem Eng China 2008;2(2):209–13.
[53] Goyal A, Pushpavanam S, Voolapalli RK. Modeling and simulation of co-gasification of coal and petcoke in a bubbling fluidized bed coal gasifier. Fuel Process Technol 2010;91(10):1296–307.
[54] Gungor A. Modeling the effects of the operational parameters on H2 composition in a biomass fluidized bed gasifier. Int J Hydrogen Energy 2011;36:6592–600.
[55] Chapman S, Cowling TG. The mathematical theory of non-uniform gases. London: Cambridge University Press; 1961.
[56] Lun CKK, Savage SB, Jefferey DJ, Chepurniy N. Kinetic theories for granular flow: inelastic particles in couette flow and slightly inelastic particles in a general flowfield. J Fluid Mech 1984;140:223.
[57] Sinclair JL, Jackson R. Gas–particle flow in a vertical pipe with particle–particle interactions. AIChE J 1989;35:1473–86.
[58] Ding J, Gidaspow D. A bubbling fluidization model using kinetic theory of granular flow. AIChE J 1990;36:523–38.
[59] Gidaspow D. Multiphase flow and fluidization. San Diego: Academic Press; 1994.
[60] Huilin L, Yurong H, Gidaspow D. Hydrodynamic modeling of binary mixture in a gas bubbling fluidized bed using kinetic theory of granular flow. Chem Eng Sci 2003;58:1197–205.
[61] Louge MY, Mastorakos E, Jenkins JT. The role of particle collisions in pneumatic transport. J Fluid Mech 1991;231:345–59.
[62] Pita JA, Sundareasan S. Gas–solids flow in vertical tubes. AIChE J 1992;37:1009–18.

[63] Hrenya CM, Sinclair JL. Effects of particle-phase turbulence in gas–solid flows. AIChE J 1997;43:853.
[64] Samuelsberg BJ, Hjertager H. Computational modeling of gas–particle flow in a riser. AIChE J 1996;42:1536–47.
[65] Nieuwland JJ, Van Sint Annaland M, Kuipers AM, Van Swaaij PM. Hydrodynamic modeling of gas–particle flows in riser reactors. AIChE J 1996;42:1569–82.
[66] Balzer G., Simonin O., Boelle A., Lavieville J. A unifying modeling approach for the numerical prediction of dilute and dense gas–solid flow. In: Proceedings of the circulating fluidized bed V, Beijing, China, 1996; MSD6.
[67] Neri A, Gidaspow D. Riser hydrodynamics: simulation using kinetic theory. AIChE J 2000;46:52–67.
[68] Armstrong LM, Gu S, Luo KH. Study of wall-to-bed heat transfer in a bubbling fluidized bed using the kinetic theory of granular flow. Int J Heat Mass Transf 2010;53:467–76.
[69] Loha C, Chattopadhyay H, Chatterjee PK. Assessment of drag models in simulating bubbling fluidized bed hydrodynamics. Chem Eng Sci 2012;75:400–7.
[70] Loha C, Chattopadhyay H, Chatterjee PK. Euler–Euler CFD modeling of fluidized bed: influence of specularity coefficient on hydrodynamic behavior. Particuology 2013;11(6):673–80.
[71] Loha C, Chattopadhyay H, Chatterjee PK. Effect of coefficient of restitution in Euler–Euler CFD simulation of fluidized bed hydrodynamics. Particuology 2014;15:170–7.
[72] Papadikis K, Gu S, Fivga A, Bridgwater AV. Numerical comparison of drag models of granular flows applied to the fast pyrolysis of biomass. Energy Fuels 2010;24:2133–45.
[73] Papadikis K, Gu S, Bridgwater AV. A CFD approach on the effect of particle size on char entrainment in bubbling fluidized bed reactor. Biomass Bioenergy 2010;34:21–9.
[74] De Wilde J, Trujillo WR. Fluid catalytic cracking in a rotating fluidized bed in a static geometry: a CFD analysis accounting for the distribution of the catalyst coke content. Powder Technol 2012;221:36–46.
[75] Syamlal M, Rogers W, O'Brien TJ. Mfix documentation theory guide. U.S. Department of Energy, Office of Fossil Energy. Technical note; 1993.
[76] Richardson JR, Zaki WN. Sedimentation and fluidization: part I. Trans Inst Chem Eng 1954;32(1):35–53.
[77] Wen CY, Yu YH. Mechanics of fluidization. Chem Eng Prog Symp Ser 1966;62:100.
[78] Syamlal M, O'Brien TJ. Computer simulation of bubbles in a fluidized bed. AIChE Symp Ser 1989;85:22–31.
[79] Ergun S. Fluid flow through packed columns. Chem Eng Prog 1952;48:89–94.
[80] Arastoopour H, Pakdel P, Adewumi M. Hydrodynamic analysis of dilute gas–solids flow in a vertical pipe. Powder Technol 1990;62(2):163–70.
[81] McKeen T, Pugsley T. Simulation and experimental validation of a freely bubbling bed of FCC catalyst. Powder Technol 2003;129:139–52.
[82] Gibilaro LG, Di Felice R, Waldram SP. Generalized friction factor and drag coefficient correlations for fluid–particle interactions. Chem Eng Sci 1985;40 (10):1817–23.
[83] Yang N, Wang W, Ge W, Li J. CFD simulation of concurrent-up gas–solid flow in circulating fluidized bed with structure-dependent drag coefficient. Chem Eng J 2003;96:71–80.
[84] Dou B, Dupont V, Williams PT. Computational fluid dynamics simulation of gas–solid flow during steam reforming of glycerol in a fluidized bed reactor. Energy Fuels 2008;22:4102–8.
[85] Dou B, Song YA. CFD approach on simulation of hydrogen production from steam reforming of glycerol in a fluidized bed reactor. Int J Hydrogen Energy 2010;35:10271–84.
[86] Papadikis K, Bridgwater AV, Gu S. CFD modelling of the fast pyrolysis of biomass in fluidised bed reactors, Part A: Eulerian computation of momentum transport in bubbling fluidised beds. Chem Eng Sci 2008;63:4218–27.
[87] Papadikis K, Gu S, Bridgwater AV. CFD modelling of the fast pyrolysis of biomass in fluidised bed reactors. Part B: heat, momentum and mass transport in bubbling fluidised beds. Chem Eng Sci 2009;64:1036–45.
[88] Xue Q, Dalluge D, Heindel TJ, Fox RO, Brown RC. Experimental validation and CFD modeling study of biomass fast pyrolysis in fluidized-bed reactors. Fuel 2012;97:757–69.
[89] Yu L, Lu J, Zhang X, Zhang S. Numerical simulation of the bubbling fluidized bed coal gasification by the kinetic theory of granular flow (KTGF). Fuel 2007;86:722–34.
[90] Wang X, Jin B, Zhong W. Three-dimensional simulation of fluidized bed coal gasification. Chem Eng Precess 2009;48:695–705.
[91] Armstrong LM, Luo K, Gu S. Effects of limestone calcinations on the gasification processes in a BFB coal gasifier. Chem Eng J 2011;168:848–60.
[92] Armstrong LM, Gu S, Luo K. Parametric study of gasification processes in BFB coal gasifier. Ind Eng Chem Res 2011;50:5959–74.
[93] Deen NG, Van Sint Annaland M, Van der Hoef MA, Kuipers JAM. Review of discrete particle modeling of fluidized beds. Chem Eng Sci 2007;62:28–44.
[94] Campbell CS, Brennen CE. Computer simulations of granular shear flows. J Fluid Mech 1985;151:167–88.
[95] Hoomans BPB, Kuipers JAM, Briels WJ, Van Swaaij WPM. Discrete particle simulation of bubble and slug formation in a two-dimensional gas–fluidised bed: a hard-sphere approach. Chem Eng Sci 1996;51(1):99–118.
[96] Hoomans BPB, Kuipers JAM, Van Swaaij WPM. Granular dynamics simulation of segregation phenomena in bubbling gas–fluidised beds. Powder Technol 2000;109(1–3):41–8.
[97] Li J, Kuipers JAM. Effect of pressure on gas–solid flow behavior in dense gas-fluidized beds: a discrete particle simulation study. Powder Technol 2002;127(2):173–84.
[98] Li J, Kuipers JAM. Gas–particle interactions in dense gas-fluidized beds. Chem Eng Sci 2003;58(3–6):711–8.
[99] He Y, Van Sint Annaland M., Deen NG, Kuipers JAM. Gas–solid two-phase turbulent flow in a circulating fluidized bed riser: an experimental and numerical study. In: Proceedings of the fifth world congress on particle technology, April 23–27, 2006, Orlando, FL, USA.
[100] Link J, Zeilstra C, Deen N, Kuipers H. Validation of a discrete particle model in a 2D spout-fluid bed using non-intrusive optical measuring techniques. Can J Chem Eng 2004;82(1):30–6.
[101] Link JM, Cuypers LA, Deen NG, Kuipers JAM. Flow regimes in a spout-fluid bed: a combined experimental and simulation study. Chem Eng Sci 2005;60 (13):3425–42.
[102] Vreman AW, Al-Tarazi M, Kuipers JAM, Van Sint Annaland M, Bokhove O. Supercritical shallow granular and hydraulic flow through a contraction: experiment, theory, and simulation. J Fluid Mech 2007;578:233–69.
[103] Dahl SR, Clelland R, Hrenya CM. The effects of continuous size distributions on the rapid flow of inelastic particles. Phys Fluids 2004;14(6):1972–84.
[104] Dahl SR, Hrenya CM. Size segregation in rapid, granular flows with continuous size distributions. Phys Fluids 2004;16(1):1–13.
[105] Dahl SR, Hrenya CM. Size segregation in gas–solid fluidized beds with continuous size distributions. Chem Eng Sci 2005;60(23):6658–73.
[106] Ouyang J, Li J. Particle-motion-resolved discrete model for simulating gas–solid fluidization. Chem Eng Sci 1999;54(13–14):2077–83.
[107] Ouyang J, Li J. Discrete simulations of heterogeneous structure and dynamic behavior in gas–solid fluidization. Chem Eng Sci 1999;54(22):5427–40.
[108] Helland E, Occelli R, Tadrist L. Numerical study of cohesive powders in a dense fluidized bed. C R Acad Sci—Ser IIb: Mec Phys Chim Astron 1999;327 (14):1397–403.
[109] Helland E, Occelli R, Tadrist L. Numerical study of cluster formation in a gas–particle circulating fluidized bed. Powder Technol 2000;110(3):210–21.
[110] Helland E, Occelli R, Tadrist L. Computational study of fluctuating motions and cluster structures in gas–particle flows. Int J Multiph Flow 2002;28 (2):199–223.
[111] Helland E, Occelli R, Tadrist L. Numerical study of cluster and particle rebound effects in a circulating fluidised bed. Chem Eng Sci 2005;60(1):27–40.
[112] Ibsen CH, Helland E, Hjertager BH, Solberg T, Tadrist L, Occelli R. Comparison of multifluid and discrete particle modelling in numerical predictions of gas particle flow in circulating fluidised beds. Powder Technol 2004;149 (1):29–41.
[113] Lun CCK. Numerical simulation of dilute turbulent gas–solid flows. Int J Multiph Flow 2000;26:1707–36.
[114] Zhou H, Flamant G, Gauthier D, Lu J. Numerical simulation of the turbulent gas–particle flow in a fluidized bed by an LES-DPM model. Chem Eng Res Des 2004;82(A7):918–26.
[115] Cundall PA, Strack ODL. A discrete numerical model for granular assemblies. Geotechnique 1979;29(1):47–65.
[116] Schafer J, Dippel S, Wolf DE. Force schemes in simulations of granular materials. J Phys I 1996;6(1):5–20.
[117] Walton OR, Braun RL. Viscosity and temperature calculations for assemblies of inelastic frictional disks. J Rheol 1986;30(5):949–80.
[118] Langston PA, Tüzün U, Heyes DM. Continuous potential discrete particle simulations of stress and velocity fields in hoppers transition from fluid to granular flow. Chem Eng Sci 1994;49(8):1259–75.
[119] Tsuji Y, Kawaguchi T, Tanaka T. Discrete particle simulation of two-dimensional fluidized bed. Powder Technol 1993;77(1):79–87.
[120] Kawaguchi T, Tanaka T, Tsuji Y. Numerical simulation of two dimensional fluidized beds using the discrete element method (comparison between the two- and three-dimensional models). Powder Technol 1998;96(2):129–38.
[121] Yu AB, Xu BH. Particle-scale modelling of gas–solid flow in fluidisation. J Chem Technol Biotechnol 2003;78(2–3):111–21.
[122] Xu BH, Yu AB, Chew SJ, Zulli P. Numerical simulation of the gas–solid flow in a bed with lateral gas blasting. Powder Technol 2000;109(1–3):13–26.
[123] Xu BH, Yu AB. Numerical simulation of the gas–solid flow in a fluidized bed by combining discrete particle method with computational fluid dynamics. Chem Eng Sci 1997;52(16):2785–809.
[124] Feng YQ, Yu AB. Assessment of model formulations in the discrete particle simulation of gas–solid flow. Ind Eng Chem Res 2004;43(26):8378–90.
[125] Feng YQ, Xu BH, Zhang SJ, Yu AB, Zulli P. Discrete particle simulation of gas fluidization of particle mixtures. AIChE J 2004;50(8):1713–28.
[126] Iwadate M, Horio M. Agglomerating fluidization of wet powders and group C powders: a numerical analysis. In: Fan LS, Knowlton T, editors. Fluidization IX. Durango, USA: Engineering Foundation; 1998. p. 293.
[127] Mikami T, Kamiya H, Horio M. Numerical simulation of cohesive powder behavior in a fluidized bed. Chem Eng Sci 1998;53(10):1927–40.
[128] Ye M, Van der Hoef MA, Kuipers JAM. A numerical study of fluidization behavior of Geldart A particles using a discrete particle model. Powder Technol 2004;139(2):129–39.
[129] Ye M, Van der Hoef MA, Kuipers JAM. The effects of particle and gas properties on the fluidization of Geldart A particles. Chem Eng Sci 2005;60(16):4567–80.
[130] Pandit JK, Wang XS, Rhodes MJ. Study of Geldart's group A behaviour using the discrete element method simulation. Powder Technol 2005;160(1):7–14.
[131] Kafui KD, Thornton C, Adams MJ. Discrete particle–continuum fluid modelling of gas–solid fluidised beds. Chem Eng Sci 2002;57(12):2395–410.

[132] Limtrakul S, Boonsrirat A, Vatanatham T. DEM modeling and simulation of a catalytic gas–solid fluidized bed reactor: a spouted bed as a case study. Chem Eng Sci 2004;59(22–23):5225–31.
[133] Kuwagi K, Mikami T, Horio M. Numerical simulation of metallic solid bridging particles in a fluidized bed at high temperature. Powder Technol 2000;109(1–3):27–40.
[134] Oevermann M, Gerber S, Behrendt F. Euler–Lagrange/DEM simulation of wood gasification in a bubbling fluidized bed reactor. Particuology 2009;7:307–16.
[135] Zhou ZY, Yu AB, Zulli P. Particle scale study of heat transfer in packed and bubbling fluidized beds. AIChE J 2009;55:868–84.
[136] Hou QF, Zhou ZY, Yu AB. Computational study of heat transfer in a bubbling fluidized bed with a horizontal tube. AIChE J 2012;58:1422–34.
[137] O'Rourke PJ. Collective drop effects on vaporizing liquid sprays. (Ph.D. thesis). Princeton University; 1981.
[138] Silaen A, Wang T. Effect of turbulence and devolatilization models on coal gasification simulation in an entrained-flow gasifier. Int J Heat Mass Transf 2010;53:2074–91.
[139] Watanabe H, Otaka M. Numerical simulation of coal gasification in entrained flow coal gasifier. Fuel 2006;85:1935–43.
[140] Gräbner M, Ogriseck S, Meyer B. Numerical simulation of coal gasification at circulating fluidised bed conditions. Fuel Process Technol 2007;88:948–58.
[141] Bruchmuller J, van Wachem BGM, Gu S, Luo KH, Brown RC. Modeling the thermochemical degradation of biomass inside a fast pyrolysis fluidized bed reactor. AIChE J 2012;58:3030–42.
[142] Andrews MJ, O'Rourke PJ. The multiphase particle-in-cell (MP-PIC) method for dense particle flow. Int J Multiph Flow 1996;22:379–402.
[143] Snider DM. An incompressible three dimensional multiphase particle-in-cell model for dense particle flows. J Comput Phys 2001;170:523–49.
[144] Snider DM. Three fundamental granular flow experiment and experiments and CPFD predictions. Powder Technol 2007;176:36–46.
[145] Smagorinsky J. General circulation experiments with the primitive equations, pat I: the basic experiment. Mon Weather Rev 1963;91:99–164.
[146] O'Rourke PJ, Snider DM. An improved collision damping time for MP-PIC calculations of dense particle flows with applications to polydisperse sedimenting beds and colliding particle jets. Chem Eng Sci 2010;65:6014–28.
[147] Harris SE, Crighton DG. Solitons solitary waves and voidage disturbances in gas-fluidized beds. J Fluid Mech 1994;266:243–76.
[148] Snider DM, Banerjee S. Heterogeneous gas chemistry in the CPFD Eulerian–Lagrangian numerical scheme (ozone decomposition). Powder Technol 2010;199:100–6.
[149] Snider DM, Clark SM, O'Rourke PJ. Eulerian–Lagrangian method for three-dimensional thermal reacting flow with application to coal gasifiers. Chem Eng Sci 2011;66:1285–95.
[150] Abbasi A, Ege PE, de Lasa HI. CPFD simulation of a fast fluidized bed steam coal gasifier feeding section. Chem Eng J 2011;174:341–50.
[151] Xie J, Zhong W, Jin B, Shao Y, Hao L. Simulation on gasification of forestry residues in fluidized beds by Eulerian–Lagrangian approach. Bioresour Technol 2012;121:36–46.
[152] Loha C, Chattopadhyay H, Chatterjee PK. Three dimensional kinetic modeling of fluidized bed biomass gasification. Chem Eng Sci 2014;109:53–64.
[153] Xie J, Zhong W, Jin B, Shao Y, Hao L. Eulerian–Lagrangian method for three-dimensional simulation of fluidized bed coal gasification. Adv Powder Technol 2013;24:382–92.